

Kent Academic Repository

Full text document (pdf)

Citation for published version

Andreano, Emanuele and Nicastri, Emanuele and Paciello, Ida and Pileri, Piero and Manganaro, Noemi and Piccini, Giulia and Manenti, Alessandro and Pantano, Elisa and Kabanova, Anna and Troisi, Marco and Vacca, Fabiola and Cardamone, Dario and De Santi, Concetta and Torres, Jonathan L. and Ozorowski, Gabriel and Benincasa, Linda and Jang, Hyesun and Di Genova, Cecilia and

DOI

<https://doi.org/10.1016/j.cell.2021.02.035>

Link to record in KAR

<https://kar.kent.ac.uk/86752/>

Document Version

Publisher pdf

Copyright & reuse

Content in the Kent Academic Repository is made available for research purposes. Unless otherwise stated all content is protected by copyright and in the absence of an open licence (eg Creative Commons), permissions for further reuse of content should be sought from the publisher, author or other copyright holder.

Versions of research

The version in the Kent Academic Repository may differ from the final published version.

Users are advised to check <http://kar.kent.ac.uk> for the status of the paper. **Users should always cite the published version of record.**

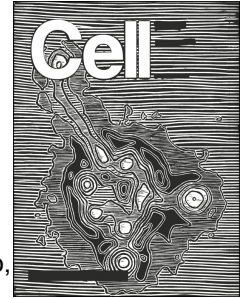
Enquiries

For any further enquiries regarding the licence status of this document, please contact:

researchsupport@kent.ac.uk

If you believe this document infringes copyright then please contact the KAR admin team with the take-down information provided at <http://kar.kent.ac.uk/contact.html>

Journal Pre-proof



Extremely potent human monoclonal antibodies from COVID-19 convalescent patients

Emanuele Andreano, Emanuele Nicastrì, Ida Paciello, Piero Pileri, Noemi Manganaro, Giulia Piccini, Alessandro Manenti, Elisa Pantano, Anna Kabanova, Marco Troisi, Fabiola Vacca, Dario Cardamone, Concetta De Santi, Jonathan L. Torres, Gabriel Ozorowski, Linda Benincasa, Hyesun Jang, Cecilia Di Genova, Lorenzo Depau, Jlenia Brunetti, Chiara Agrati, Maria Rosaria Capobianchi, Concetta Castilletti, Arianna Emiliozzi, Massimiliano Fabbiani, Francesca Montagnani, Luisa Bracci, Giuseppe Sautto, Ted M. Ross, Emanuele Montomoli, Nigel Temperton, Andrew B. Ward, Claudia Sala, Giuseppe Ippolito, Rino Rappuoli

PII: S0092-8674(21)00224-5

DOI: <https://doi.org/10.1016/j.cell.2021.02.035>

Reference: CELL 11898

To appear in: *Cell*

Received Date: 24 November 2020

Revised Date: 25 January 2021

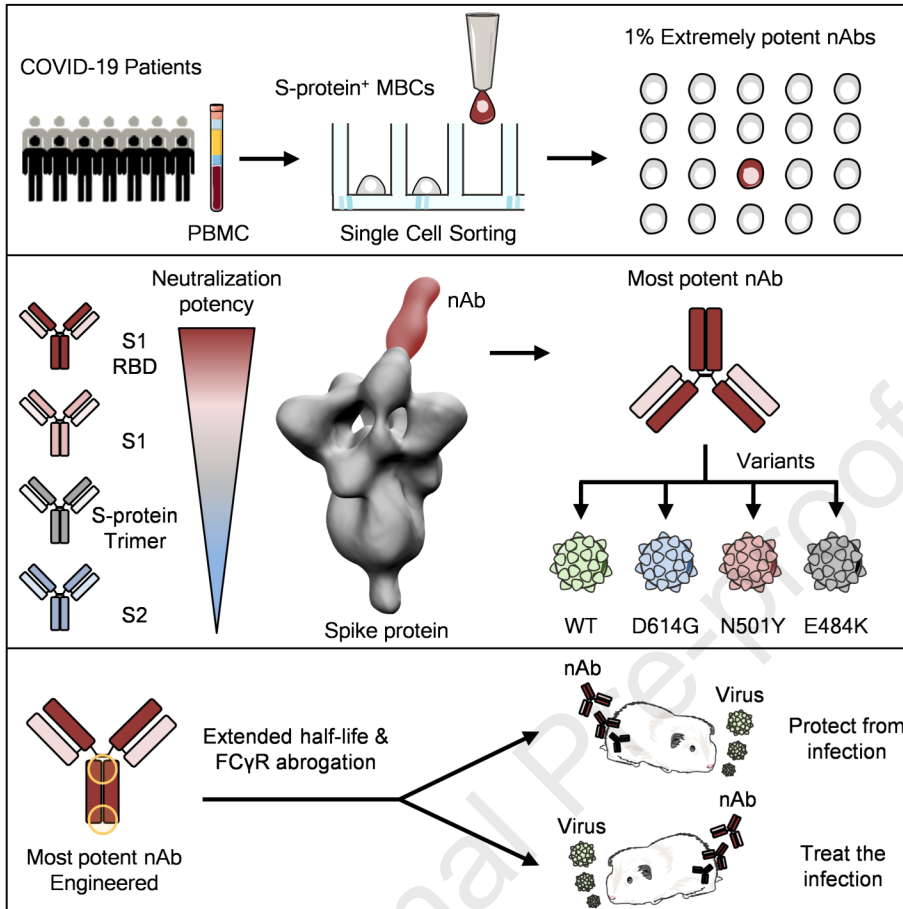
Accepted Date: 16 February 2021

Please cite this article as: Andreano, E., Nicastrì, E., Paciello, I., Pileri, P., Manganaro, N., Piccini, G., Manenti, A., Pantano, E., Kabanova, A., Troisi, M., Vacca, F., Cardamone, D., De Santi, C., Torres, J.L., Ozorowski, G., Benincasa, L., Jang, H., Di Genova, C., Depau, L., Brunetti, J., Agrati, C., Capobianchi, M.R., Castilletti, C., Emiliozzi, A., Fabbiani, M., Montagnani, F., Bracci, L., Sautto, G., Ross, T.M., Montomoli, E., Temperton, N., Ward, A.B., Sala, C., Ippolito, G., Rappuoli, R., Extremely potent human monoclonal antibodies from COVID-19 convalescent patients, *Cell* (2021), doi: <https://doi.org/10.1016/j.cell.2021.02.035>.

This is a PDF file of an article that has undergone enhancements after acceptance, such as the addition of a cover page and metadata, and formatting for readability, but it is not yet the definitive version of record. This version will undergo additional copyediting, typesetting and review before it is published in its final form, but we are providing this version to give early visibility of the article. Please note that,

during the production process, errors may be discovered which could affect the content, and all legal disclaimers that apply to the journal pertain.

© 2021 Elsevier Inc.



Extremely potent human monoclonal antibodies from COVID-19 convalescent patients

Emanuele Andreano^{1†}, Emanuele Nicastrì^{4†}, Ida Paciello¹, Piero Pileri¹, Noemi Manganaro¹, Giulia Piccini², Alessandro Manenti^{2,3}, Elisa Pantano¹, Anna Kabanova^{1,11}, Marco Troisi^{1,9}, Fabiola Vacca^{1,9}, Dario Cardamone^{1,10}, Concetta De Santi¹, Jonathan L. Torres¹⁶, Gabriel Ozorowski¹⁶, Linda Benincasa³, Hyesun Jang¹³, Cecilia Di Genova¹⁵, Lorenzo Depau¹², Jlenia Brunetti¹², Chiara Agrati⁴, Maria Rosaria Capobianchi⁴, Concetta Castilletti⁴, Arianna Emiliozzi^{5,6}, Massimiliano Fabbiani⁶, Francesca Montagnani^{5,6}, Luisa Bracci¹², Giuseppe Sautto¹³, Ted M. Ross^{13,14}, Emanuele Montomoli^{2,3,7}, Nigel Temperton¹⁵, Andrew B. Ward¹⁶, Claudia Sala¹, Giuseppe Ippolito⁴, Rino Rappuoli^{1,8,17,*}

¹Monoclonal Antibody Discovery (MAD) Lab, Fondazione Toscana Life Sciences, Siena, Italy

²VisMederi S.r.l, Siena, Italy

³VisMederi Research S.r.l., Siena, Italy

⁴National Institute for Infectious Diseases Lazzaro Spallanzani, IRCCS, Rome, Italy

⁵Department of Medical Biotechnologies, University of Siena, Siena, Italy

⁶Department of Medical Sciences, Infectious and Tropical Diseases Unit, University Hospital of Siena, Siena, Italy

⁷Department of Molecular and Developmental Medicine, University of Siena, Siena, Italy

⁸Faculty of Medicine, Imperial College, London, United Kingdom

⁹Department of Biotechnology, Chemistry and Pharmacy, University of Siena, Siena, Italy

¹⁰University of Turin, Turin, Italy

¹¹Tumour Immunology Unit, Fondazione Toscana Life Sciences, Siena, Italy

¹²MedBiotech Hub and Competence Center, Department of Medical Biotechnologies, University of Siena

¹³Center for Vaccines and Immunology, University of Georgia, Athens, GA 30602, USA.

¹⁴Department of Infectious Diseases, University of Georgia, Athens, GA 30602, USA.

¹⁵Viral Pseudotype Unit, Medway School of Pharmacy, University of Kent, Chatham, UK

¹⁶Department of Integrative Structural and Computational Biology, The Scripps Research Institute, La Jolla, CA 92037

¹⁷Lead contact

[†]These authors contributed equally in sample processing and patient enrolment respectively.

*To whom correspondence should be addressed: Dr. Rino Rappuoli rino.r.rappuoli@gsk.com (R.R.)

35 **SUMMARY**

36 Human monoclonal antibodies are safe, preventive and therapeutic tools, that can be rapidly
37 developed to help restore the massive health and economic disruption caused by the coronavirus
38 disease 2019 (COVID-19) pandemic. By single cell sorting 4,277 SARS-CoV-2 spike protein
39 specific memory B cells from 14 COVID-19 survivors, 453 neutralizing antibodies were identified.
40 The most potent neutralizing antibodies recognized the spike protein receptor binding domain,
41 followed in potency by antibodies that recognize the S1 domain, the spike protein trimer and the S2
42 subunit. Only 1.4% of them neutralized the authentic virus with a potency of 1-10 ng/mL. The most
43 potent monoclonal antibody, engineered to reduce the risk of antibody dependent enhancement
44 and prolong half-life, neutralized the authentic wild type virus and emerging variants containing
45 D614G, E484K and N501Y substitutions. Prophylactic and therapeutic efficacy in the hamster
46 model was observed at 0.25 and 4 mg/kg respectively in absence of Fc-functions.

47 INTRODUCTION

48 The impact of the severe acute respiratory syndrome coronavirus 2 (SARS-CoV-2) pandemic, with
49 more than 100 million cases, over 2 million deaths, an estimated cost of 16 trillion US dollars to the
50 USA economy (Cutler and Summers, 2020) and 45 million people filing unemployment in the
51 United States alone, is unprecedented (Aratani, 2020).

52 Vaccines and drugs against SARS-CoV-2 have recently received emergency use authorization
53 (EUA) by the Food and Drug Administration (FDA) for prevention and treatment of coronavirus
54 disease 2019 (COVID-19) (FDA, 2021, FDA, 2020).

55 In spite of this, it is predictable that waves of infection will continue to spread globally and it is likely
56 to be followed by additional waves over the next few years. This is supported by the emergence of
57 new SARS-CoV-2 variants in the United Kingdom, South Africa, Brazil and Japan (CDC, 2021).

58 It is therefore imperative to quickly develop, in parallel to vaccines, therapeutic tools against SARS-
59 CoV-2 and its variants. Among the many therapeutic options available, human monoclonal
60 antibodies (mAbs) can be developed in the shortest time frame. In fact, the extensive clinical
61 experience with the safety of more than 50 commercially available mAbs approved to treat cancer,
62 inflammatory and autoimmune disorders, provides high confidence of their safety (Wellcome,
63 2020). These advantages, combined with the urgency of the SARS-CoV-2 pandemic, support and
64 justify an accelerated regulatory pathway. In addition, the long industrial experience in developing
65 and manufacturing mAbs decreases risks usually associated with technical development of
66 investigational products. Finally, the incredible technical progress in this field allows shortening of
67 conventional timelines and enables a path from discovery to proof of concept trials within 5-6
68 months (Kelley, 2020). A key example is the Ebola case, where mAbs were developed faster than
69 vaccines or other drugs (Kupferschmidt, 2019) becoming the first therapeutic intervention
70 recommended by the World Health Organization (WHO) and approved by the Food and Drug
71 Administration (FDA) (Mullard, 2020).

72 During the first months of this pandemic many groups have been active in isolating and
73 characterizing human monoclonal antibodies from COVID-19 convalescent patients or from
74 humanized mice and some of them have been progressing quickly to clinical trials for the

75 prevention and cure of SARS-CoV-2 infection (Shi et al., 2020, Hansen et al., 2020, Hsieh et al.,
76 2020, Pinto et al., 2020, Zost et al., 2020a, Zost et al., 2020b, Rogers et al., 2020, Alsoussi et al.,
77 2020). Few of them are already in phase III clinical trials and reported promising preliminary
78 results. Two of them received the Emergency Use Authorization from the FDA (Lilly, 2020,
79 Regeneron, 2020).

80 All these antibodies neutralize SARS-CoV-2 infection by binding to the spike glycoprotein (S-
81 protein), a trimeric class I viral fusion protein which mediates virus entry into host cells by engaging
82 with the human angiotensin converting enzyme 2 (hACE2) and cellular heparan sulfate as
83 receptors (Clausen et al., 2020). The S-protein exists in a metastable pre-fusion conformation and
84 in a stable post-fusion form (Wang et al., 2020, Walls et al., 2020, Schäfer et al., 2020). Each S-
85 protein monomer is composed of two distinct regions, the S1 and S2 subunits. The S1 subunit
86 contains the receptor binding domain (RBD) which is responsible for the interaction with hACE2
87 and heparan sulfate on host cell membranes triggering the destabilization of the prefusion state of
88 the S-protein and consequent transition into the post-fusion conformation. This event results in the
89 entry of the virus particle into the host cell and the onset of infection (Wrapp et al., 2020, Walls et
90 al., 2020, Tay et al., 2020, Zou et al., 2020).

91 As for other mAbs in the field of infectious diseases (Hooft van Huijsduijnen et al., 2020, Sparrow et
92 al., 2017), the dose of mAbs so far used in clinical trials against SARS-CoV-2 is high, ranging from
93 500 to 8,000 mgs (NCT04411628; NCT04427501; NCT04441918; NCT04425629; NCT04426695;
94 NCT04452318). The high dose poses two important limits to the application of mAbs in the
95 infectious diseases field. Firstly, the high dosage has cost-associated implications and it only
96 allows for intravenous delivery making this therapeutic intervention extremely costly and therefore
97 available almost exclusively in high-income countries. Indeed, the high price of this intervention has
98 been a barrier to the global access of mAbs and their use to other fields such as infectious
99 diseases. A solution would be the development of extremely potent mAbs that can be used at lower
100 dosages leading to cost reductions and that can be delivered via intramuscular or subcutaneous
101 injections. A first example is the respiratory syncytial virus (RSV) case, where a potent mAb has

102 recently shown its therapeutic effect in premature infants after only one intramuscular injection of
103 50 mg (Griffin et al., 2020).

104 The second limit of mAbs in the field of infectious diseases is the risk of antibody dependent
105 enhancement (ADE) of disease which is usually mediated by the binding of the fragment
106 crystallizable region (Fc) portion of the antibody to Fc gamma receptors (FcγRs) expressed by
107 immune cells (Lee et al., 2020). ADE has been clearly demonstrated in the case of SARS-CoV,
108 RSV and dengue viruses and the theoretical risk has been raised in the case of SARS-CoV-2 (Lee
109 et al., 2020, Katzelnick et al., 2017, Arvin et al., 2020).

110 In this work we pushed the limits of mAb application to fight infectious diseases by selecting
111 extremely potent antibodies with the aim of using them at low dosage, to make them affordable and
112 conveniently delivered by intramuscular injection. In addition, we mitigated the risk of ADE by
113 engineering their Fc region. Despite complete lack of Fc-receptor binding and Fc-mediated cellular
114 activities, engineered mAbs were able to prevent and treat SARS-CoV-2 infection in golden Syrian
115 hamster at a concentration of 0.25 and 4 mg/kg respectively. These antibodies have the potential
116 to globally extend the access and affordability of this important medical tool.

117 **RESULTS**118 **Isolation and characterization of S-protein specific antibodies from SARS-CoV-2 convalescent**
119 **patients**

120 To retrieve mAbs specific for SARS-CoV-2 S-protein, peripheral blood mononuclear cells (PBMCs)
121 from fourteen COVID-19 convalescent patients enrolled in this study were collected and stained
122 with fluorescently labelled S-protein trimer to identify antigen specific memory B cells (MBCs).
123 Figure 1 summarizes the overall experimental strategy. The gating strategy described in Figure
124 S1A was used to single cell sort, into 384-well plates, IgG⁺ and IgA⁺ MBCs binding to the SARS-
125 CoV-2 S-protein trimer in its prefusion conformation. The sorting strategy aimed to specifically
126 identify class-switched MBCs (CD19⁺CD27⁺IgD⁻IgM⁻) to identify only memory B lymphocytes that
127 underwent maturation processes. A total of 4,277 S-protein-binding MBCs were successfully
128 retrieved with frequencies ranging from 0.17% to 1.41% (Table S1). Following the sorting
129 procedure, S-protein⁺ MBCs were incubated over a layer of 3T3-CD40L feeder cells in the
130 presence of IL-2 and IL-21 stimuli for two weeks to allow natural production of immunoglobulins
131 (Huang et al., 2013). Subsequently, MBC supernatants containing IgG or IgA were tested for their
132 ability to bind either the SARS-CoV-2 S-protein trimer in its prefusion conformation or the S-protein
133 S1 + S2 subunits (Figure 2A and Figure S2B) by enzyme linked immunosorbent assay (ELISA). A
134 panel of 1,731 mAbs specific for the SARS-CoV-2 S-protein were identified showing a broad range
135 of signal intensities (Figure 2A; Table S1).

136
137 **Identification of S-protein specific mAbs able to neutralize SARS-CoV-2**

138 The 1,731 supernatants containing S-protein specific mAbs, were screened *in vitro* for their ability
139 to block the binding of the streptavidin-labelled S-protein to Vero E6 cell receptors and for their
140 ability to neutralize authentic SARS-CoV-2 virus by *in vitro* microneutralization assay. In the
141 neutralization of binding (NoB) assay, 339 of the 1,731 tested (19.6%) S-protein specific mAbs
142 were able to neutralize the antigen/receptor binding showing a broad array of neutralization
143 potency ranging from 50% to 100% (Table S1 and Figure S2C).

144 As for the authentic virus neutralization assay, supernatants containing naturally produced IgG or
145 IgA were tested for their ability to protect the layer of Vero E6 cells from the cytopathic effect
146 triggered by SARS-CoV-2 infection. To increase the throughput of our approach, supernatants
147 were tested at a single point dilution and to increase the sensitivity of our first screening a viral titer
148 of 25 TCID₅₀ was used. For this screening mAbs were classified as neutralizing, partially
149 neutralizing and non-neutralizing based on their complete, partial or absent ability to prevent the
150 infection of Vero E6 cells respectively. Out of 1,731 mAbs tested in this study, a panel of 453
151 (26.2%) mAbs neutralized the authentic virus and prevented infection of Vero E6 cells (Table S1).
152 The percentage of partially neutralizing mAbs and neutralizing mAbs (nAbs) identified in each
153 donor was extremely variable ranging from 2.6 - 29.7% and 2.8 - 26.4% respectively (Figure 2B
154 and Table S2). The majority of nAbs were able to specifically recognize the S-protein S1 domain
155 (57.5%; N=244) while 7.3% (N=53) of nAbs were specific for the S2 domain and 35.2% (N=156)
156 did not recognize single domains but only the S-protein in its trimeric conformation (Figure S2A;
157 Table S3). From the panel of 453 nAbs, we recovered the heavy and light chain variable regions of
158 220 nAbs which were expressed as full length IgG1 using the transcriptionally active PCR (TAP)
159 approach to characterize their neutralization potency against the live virus at 100 TCID₅₀. The vast
160 majority of nAbs identified (65.9%; N=145) had a low neutralizing potency and required more than
161 500 ng/mL to achieve 100% inhibitory concentration (IC₁₀₀). A smaller fraction of the antibodies had
162 an intermediate neutralizing potency (23.6%; N=52) requiring between 100 and 500 ng/mL to
163 achieve the IC₁₀₀, while 9.1% (N=20) required between 10 and 100 ng/mL. Finally, only 1.4% (N=3)
164 of the expressed nAbs were classified as extremely potent nAbs, showing an IC₁₀₀ lower than 10
165 ng/mL (Figure 2C and Figure S2B; Table S4).

166 167 **SARS-CoV-2 neutralizing antibodies can be classified into four groups**

168 Based on the first round of screening, 14 nAbs were selected for further characterization. All nAbs
169 were able to bind the SARS-CoV-2 S-protein in its trimeric conformation (Figure 3A). The mAbs
170 named J08, I14, F05, G12, C14, B07, I21, J13 and D14 were also able to specifically bind the S1
171 domain (Figure 3B). The nAbs named H20, I15, F10 and F20 were not able to bind single S1 or S2

172 domains but only the S-protein in its trimeric state, while the nAb L19 bound only the S2 subunit
173 (Figure 3B - C). Among the group of S1 specific nAbs only J08, I14, F05, G12, C14 and B07 were
174 able to bind the S1-RBD and to strongly inhibit the interaction between the S-protein and Vero E6
175 receptors showing a half maximal effective concentration (EC_{50}) at the NoB assay of 78.6, 15.6 and
176 68.5 ng/mL for J08-MUT, I14-MUT and F05-MUT respectively (Figure S3A - B). On the other hand,
177 I21, J13 and D14, despite showing S1 binding specificity, did not show any binding to the RBD and
178 NoB activity (Figure S3A). Based on this description four different groups of nAbs against SARS-
179 CoV-2 were identified. The first group (Group I) is composed of S1-RBD specific nAbs (J08, I14,
180 F05, G12, C14 and B07) which showed neutralization potency against the authentic wild type (WT),
181 the D614G variant and the emerging variant recently isolated in the UK B.1.1.7. S1-RBD specific
182 nAbs showed a neutralizing potency ranging from 3.9 to 157.5 ng/mL (Figure 3D - I; Table S5) and
183 picomolar affinity to the S-protein with a KD ranging from 0.2 to $4.6 E^{-10}M$ (Figure S4). In addition to
184 the D616G and the B.1.1.7 variants, the S1-RBD specific nAb J08 showed also to neutralize
185 SARS-CoV-2 variants containing the E484K mutation (Andreano et al., 2020). The second group
186 (Group II) included S1-specific nAbs that did not bind the RBD (I21, J13 and D14). These
187 antibodies also showed good neutralization potency ranging from 99.2 to 500.0 ng/mL (Figure 3D -
188 I; Table S5) but inferior to that of S1-RBD directed nAbs. One antibody from this group was not
189 able to neutralize the B.1.1.7 variant (I21). The third group (Group III) is composed by antibodies
190 able to bind the S-protein only in its whole trimeric conformation (H20, I15, F10 and F20).
191 Antibodies belonging to this group showed lower affinity to the S-protein trimer (KD $64.0 E^{-10}M$ -
192 $757.0 E^{-10}M$) compared to Group I nAbs and medium neutralization potencies ranging from 155.0 to
193 492.2 ng/mL against the authentic WT and D614G (Figure 3D - I; Table S5; Figure S4). On the
194 other hand, only one S-protein specific nAb (D21) showed moderate neutralization activity against
195 the B.1.1.7 with an IC_{100} of 500.0 ng/mL. Three S-protein specific nAbs (I15, F10 and F20) did not
196 show any functional activity against this latter variant (Figure 3D - I; Table S5). The fourth and final
197 group (Group IV) is composed of antibodies that exclusively recognized the S2 domain. Different
198 antibodies with similar properties were identified for the Group IV but only the nAb L19 is shown.
199 The Group IV nAb L19 shows the lowest neutralization potency with 19.8 μ g/mL for the authentic

200 WT, 12.5 µg/mL against the D614G, and 9.9 µg/mL against the B.1.1.7 variant (Figure 3D - I; Table
201 S5).

202 All the antibodies described above were also tested for their ability to cross-neutralize other human
203 coronavirus strains. nAbs were tested against lentiviral pseudotypes expressing the SARS-CoV-2,
204 SARS-CoV-2 D614G, SARS-CoV and Middle East Respiratory Syndrome (MERS-CoV) spike
205 protein on their viral membrane surface. Neutralization activity was shown against SARS-CoV-2
206 and D614G pseudotypes and therefore confirming previous data. None of the antibodies herein
207 reported were able to cross-neutralize other coronavirus species (Figure S5).

208

209 **Different pathogen vulnerability regions identified on the S-protein**

210 The fourteen selected nAbs were further characterized by a competition assay that allowed
211 speculation on the S-protein regions recognized by these antibodies. Briefly, beads were coated
212 with SARS-CoV-2 trimeric S-protein and incubated with a primary unlabeled antibody in order to
213 saturate the binding site on the antigen surface. Following the first incubation step a secondary
214 Alexa-647 labeled antibody was incubated with the antigen/unlabeled-mAb complex. If the
215 secondary labeled-antibody did not recognize the same epitope as the primary unlabeled-mAb a
216 fluorescent signal would be detected when tested by flow cytometry. Through this assay, we
217 observed that all Group I nAbs competed amongst themselves for binding to the S-protein RBD,
218 indicating that these antibodies possibly clash against each other and recognize a similar epitope
219 region. All Group II nAbs, showed a different competition profiles and competed with Group II and
220 Group III nAbs. These results confirmed that Group III antibodies can recognize various regions on
221 the S-protein surface as they compete with themselves as well as with antibodies belonging to
222 Group II. Interestingly, nAbs belonging to Group II also competed with the B07 RBD-directed
223 antibody and thereby suggesting that this latter nAb may have a different binding orientation
224 compared to other nAbs included in the Group I. Finally, the Group IV nAb L19 did not compete
225 with any of the other groups identified in this study suggesting that this class of nAbs recognize a
226 distant epitope region as compared to Group I - II and III nAbs (Figure 4A - B)

227

228 Genetic characterization of SARS-CoV-2 nAbs

229 The genes encoding the heavy and light chains of the 14 selected nAbs, were sequenced and their
230 IGHV and IGKV genes compared with publicly available SARS-CoV-2 neutralizing antibody
231 sequences (Figure 5A - B). Four nAbs used one of the most predominant heavy chain V genes for
232 SARS-CoV-2 nAbs (IGHV1-69), while three nAbs used one of the least representative heavy chain
233 V genes (IGHV1-24). Other two nAbs, employed the most common germline observed for SARS-
234 CoV-2 nAbs which is IGHV3-53 (Figure 5A) (Yuan et al., 2020). Interestingly, while IGHV1-69 and
235 IGHV1-24 accommodate IGHJ diversity, nAbs belonging to the IGHV3-53 gene family only showed
236 recombination with the IGHJ6 gene (Table S6). The heavy chain V genes somatic hypermutation
237 level and complementary determining region 3 (H-CDR3) length were also evaluated. Our selected
238 nAbs displayed a low level of somatic mutations when compared to the inferred germlines with
239 sequence identities ranging from 95.6 to 99.3% (Figure 5C left panel; Table S6) confirming what
240 was observed in previous publications (Pinto et al., 2020, Zost et al., 2020b, Rogers et al., 2020,
241 Griffin et al., 2020). The H-CDR3 length spanned from 7 to 21 amino acids (aa) with the majority of
242 the antibodies (N=6; 42.0%) having a length of 14 to 16 aa that is slightly bigger than previously
243 observed (Figure 5C right panel; Table S6). All of our nAbs used the κ -chain and the majority of
244 them used the common genes IGKV1-9 and IGKV3-11 (N=6; 42.0%) (Figure 5B; Table S6). The
245 level of IGKV somatic hypermutation was extremely low for light chains showing a percentage of
246 sequence identities ranging from 94.3 to 98.9% (Figure 5D left panel; Table S6). The light chain
247 CDR3 (L-CDR3) length were ranging from 5 to 10 aa which is in line with what was previously
248 observed for SARS-CoV-2 nAbs (Figure 5D right panel; Table S6). When paired heavy and light
249 chain gene analysis was performed, IGHV1-69 derived nAbs were found to rearrange exclusively
250 with IGKV3 gene family while IGHV1-24 derived nAbs accommodate light chain diversity (Table
251 S6). Of note, some of our candidates showed unique heavy and light chain pairing when compared
252 to the public SARS-CoV-2 nAb repertoire. Particularly, five different heavy and light chain
253 rearrangements not previously described for nAbs against SARS-CoV-2 were identified. These
254 included the IGHV1-24;IGKV1-9, IGHV1-24;IGKV3-15, IGHV1-46;IGKV1-16, IGHV3-30;IGKV1-9,
255 IGHV3-53;IGKV1-17 (Figure 5E).

256 Fc-engineering of candidate nAbs to abrogate Fc receptor binding and extend half-life

257 Antibody-dependent enhancement (ADE) of disease, is a potential clinical risk following
258 coronavirus infection (Lee et al., 2020). Therefore, to optimize the suitability for clinical
259 development and reduce the risk of ADE, five different point mutations were introduced in the
260 constant region (Fc) of the three most potent nAbs (J08, I14 and F05) which were renamed J08-
261 MUT, I14-MUT and F05-MUT. The first two point mutations (M428L/N434S) were introduced to
262 enhance antibody half-life and to increase tissue distribution and persistence (Zalevsky et al.,
263 2010, Gaudinski et al., 2018, Pegu et al., 2017). The remaining three point mutations
264 (L234A/L235A/ P329G) were introduced to reduce antibody dependent functions such as binding to
265 FcγRs and cell-based activities (Schlothauer et al., 2016).

266 To confirm the lack of FcγR binding as well as the extended half-life, a beads-based Luminex
267 assay was performed. Briefly the beads were coated with SARS-CoV-2 S-protein RBD. Antibodies
268 were tested at eight-point dilutions and the binding was detected with FcγR2A and neonatal Fc
269 receptor (FcRn) at pH6.2 and 7.4. The FcγR2A was selected as it is predominantly expressed on
270 the surface of phagocytic cells (such as monocytes, macrophages and neutrophils) and is
271 associated with phagocytosis of immune complexes and antibody-opsionized targets (Ackerman et
272 al., 2013). On the other hand, FcRn, which is highly expressed on endothelial cells and circulating
273 monocytes, was selected as it is responsible for the recycling and serum half-life of IgG in the
274 circulation (Mackness et al., 2019). This latter receptor was shown to possess a tighter binding at
275 lower pH (e.g. pH 6.2) compared to a physiological pH (e.g. pH 7.4) (Booth et al., 2018). Results
276 shown in Figure S6 demonstrate that binding to the FcγR2A was completely abrogated for the
277 mutated version of candidate nAbs (J08-MUT, I14-MUT and F05-MUT) compared to their
278 respective wild type (WT) versions (J08, I14 and F05) and controls (CR3022 and unrelated protein)
279 (Figure S6A). Furthermore, Fc-engineered antibodies showed increased binding activity to the
280 FcRn at both pH 6.2 and 7.4 compared to their WT counterpart (Figure S6B - C). Finally, to
281 evaluate the lack of Fc-mediated cellular activities by our three candidate nAbs, the antibody-
282 dependent neutrophil phagocytosis (ADNP) and antibody-dependent NK cell activation (ADNK)
283 were evaluated (Butler et al., 2019, Ackerman et al., 2016, Karsten et al., 2019, Boudreau et al.,

284 2020). For the ADNP assay, primary human neutrophils were used to detect antibody binding to
285 SARS-CoV-2 S-protein RBD coated beads, while ADNK activity was evaluated by using primary
286 human NK cells and detecting the release of the proinflammatory cytokine interferon gamma (IFN-
287 γ). Complete abrogation of both ADNP and ADNK was observed for all three Fc-engineered
288 candidate nAbs compared to their WT versions and control antibody (CR3022), thus confirming the
289 lack of Fc-mediated cellular activities (Figure S6D - E).

290

291 **Potency and autoreactivity evaluation of Fc-engineered candidates**

292 The three engineered antibodies were tested to confirm their binding specificity and neutralization
293 potency against both the WT, the widespread SARS-CoV-2 D614G mutant and the emerging
294 variant B.1.1.7 (Korber et al., 2020, CDC, 2021) to evaluate their cross-neutralization ability. The
295 three engineered nAbs maintained their S1-domain binding specificity and extremely high
296 neutralization potency with J08-MUT and F05-MUT being able to neutralize both the WT and the
297 D614G variant with an IC_{100} lower than 10 ng/mL (both at 3.9 ng/mL for the WT and the D614G
298 strains) (Figure S6F - K; Table S5). The antibody J08-MUT also showed extreme neutralization
299 potency against emerging variants as it was able to neutralize the B.1.1.7 with an identical IC_{100}
300 compared to the WT virus (Figure S6K; Table S5) and has also showed to neutralize variants that
301 include the E484K mutation (Andreano et al., 2020).

302 Since it has been reported that SARS-CoV-2 elicited antibodies that can cross-react with human
303 tissues, cytokines, phospholipids and phospholipid-binding proteins (Zuo et al., 2020, Bastard et
304 al., 2020, Kreer et al., 2020), the three candidate mAbs in both their WT and MUT versions were
305 tested through an indirect immunofluorescent assay against human epithelial type 2 (HEp-2) cells
306 which expose clinically relevant proteins to detect autoantibody activities (Figure S7A). As reported
307 in Figure S7B, the positive control presents a different range of detectable signals based on the
308 initial dilution steps (from bright-green at 1:1 to very dim-green at 1:100). Among all samples
309 tested, only F05 showed moderate level of autoreactivity to human cells while no signal could be
310 measured for the other antibodies (Figure S7B).

311

312 Structural analyses of candidate nAbs

313 Single particle negative stain electron microscopy (nsEM) was used to visualize a stabilized SARS-
314 2-CoV-6P-Mut7 spike protein in complex with three separate Fabs: J08, I14 and F05. This
315 recombinant, soluble spike protein primarily exhibits 3 RBD's "down" but can switch to RBD "up"
316 conformation with antibody bound. Inspection of the 2D class averages revealed a mixed
317 stoichiometry of unbound spike protein, 1 Fab bound, and 2 Fab bound classes, which allowed for
318 3D refinements of each (Figure 6A). The three different Fabs bind to the RBD in the "up"
319 conformation, although at different angles and rotations, likely due to the flexibility of the RBD.
320 Model docking of PDB 7BYR (one RBD "up" bound to antibody) shows that the fabs overlap with
321 the receptor binding motif (RBM), and therefore are positioned to sterically block receptor hACE2
322 engagement (Figure 6B). To determine the epitope, heavy chain (HC) and light chain (LC)
323 sequences of Fabs J08, I14, and F05 were used to create synthetic models for docking into the
324 nsEM maps. Based on the docking, we predicted that a loop containing residues 477 to 489
325 (STPCNGVEGFNCY) appeared to be involved in the binding specifically with residue F486
326 extending into a cavity that is in the middle of the HC and LC of each antibody.

327
328 J08-MUT prevents SARS-CoV-2 infection in the golden Syrian hamster

329 The golden Syrian hamster model has been widely used to assess monoclonal antibody
330 prophylactic and therapeutic activities against SARS-CoV-2 infection. This model has shown to
331 manifest severe forms of SARS-CoV-2 infection mimicking more closely the clinical disease
332 observed in humans (Baum et al., 2020, Imai et al., 2020, Rogers et al., 2020, Sia et al., 2020). We
333 designed a prophylactic study in golden Syrian hamster to evaluate the efficacy of J08-MUT in
334 preventing SARS-CoV-2 infection. For this study 30 hamsters were divided into 5 arms (six animals
335 each) which received, J08-MUT at 4, 1 and 0.25 mg/kg via intraperitoneal injection. Placebo and
336 IgG1 isotype control groups were included in the study which received a saline solution and an
337 anti-influenza antibody at the concentration of 4 mg/kg respectively. The J08-MUT at 4 mg/kg
338 group and the 1 and 0.25 mg/kg groups were tested in two independent experiments. The IgG1
339 isotype control group was tested in parallel with the J08-MUT 4 mg/kg group while the placebo is
340 an average of the two experiments. Animals were challenged with 100 μ L of SARS-CoV-2 solution

341 (5 x 10⁵ PFU) via intranasal distillation twenty four hours post-administration of the antibody. Three
342 hamsters per group were sacrificed at three days post-infection while the remaining animals were
343 culled at day 8 (Figure 7A). Body weight change was daily evaluated and considered as a proxy for
344 disease severity. Animals in the control group and those that received the IgG1 isotype antibody
345 lost more than 5% of their original body weight from day 1 to day 6 and then stabilized. These data
346 are in line with previously published data of SARS-CoV-2 infection in a golden Syrian hamster
347 model (Kreye et al., 2020, Liu et al., 2020). In marked contrast, in the prophylactic study, all
348 animals that received J08-MUT were significantly protected from weight loss. Protection was
349 present at all J08-MUT concentrations and was dose dependent (Figure 7B). When J08-MUT was
350 administered at 4 mg/kg we observed protection from SARS-CoV-2 infection and only a minimal
351 weight loss (average -1.8% of body weight) was noticed one day post viral challenge. A higher
352 body weight loss was observed 1 day post infection in hamsters that received J08-MUT at 1 mg/kg
353 (from -1.8% to -3.3%) and 0.25 mg/kg (from -1.8% to -4.7%). In the J08-MUT 4 mg/kg group all
354 animals quickly recovered and reached their initial weight by day 3. From day 4 on all hamsters
355 gained weight increasing up to 5% from their initial body weight. Hamsters that received the 1 and
356 0.25 mg/kg dosages completely recovered their initial body weight at day 6 and 8 respectively.
357 Hamsters in the control groups did not recover their initial body weight and at day 8 still showed
358 around 5% of weight loss (Figure 7B). The prophylactic activity of J08-MUT was also reflected in
359 the complete absence of viral titer in the lung tissue at three days post-infection in all hamsters that
360 received J08-MUT at 4 and 1 mg/kg and also in two out of three hamsters that received J08-MUT
361 at 0.25 mg/kg. On the other hand, hamsters that received the IgG1 isotype control or in the placebo
362 group showed a significantly higher viral titer (Figure 7D).

363 Finally, we performed an ELISA assay to detect the presence of human IgG in hamster sera. All
364 samples that received J08-MUT or the IgG1 isotype control showed detectable human IgGs in the
365 sera in a dose-dependent fashion, while no human IgGs were detected in the placebo group
366 (Figure 7E - F). Human IgGs were detected at three and up to seven days post infection (Figure 7E
367 - F).

368

369 J08-MUT therapy of SARS-CoV-2 infection in the golden Syrian hamster

370 For the therapeutic study, 3 groups of 6 animals each were used to evaluate the ability of J08-MUT
371 to treat SARS-CoV-2 infection in the golden Syrian hamster model. One group received J08-MUT
372 via intraperitoneal injection at 4 mg/kg and the other two groups received placebo and 4mg/kg IgG1
373 isotype control respectively. The experiment was performed in parallel with the initial prophylactic,
374 study where J08-MUT was administered at 4 mg/kg, and the two control groups. Animals were
375 challenged with 100 μ L of SARS-CoV-2 solution (5×10^5 PFU) via intranasal distillation twenty four
376 hours prior to the administration of the antibody. Three hamsters per group were sacrificed at three
377 days post-infection while the remaining animals were culled at day 12 (Figure 7A). Despite J08-
378 MUT and control groups showed a similar trend in weight loss in the first four days post-infection,
379 the treatment group showed a significantly quicker weight recovery (Figure 7C). At day 12, only
380 hamsters that received J08-MUT recovered the initial body weight (Figure 7C). When we analyzed
381 the viral titer in lung tissues we observed complete absence of the virus at day 3 in all the hamsters
382 treated with J08-MUT at 4 mg/kg while animals that received the IgG1 isotype control or in the
383 placebo group showed a significantly higher viral titer (Figure 7G). To evaluate the presence of
384 human antibodies in hamster sera, we performed an ELISA assay. All samples that received J08-
385 MUT or the IgG1 isotype control showed detectable human IgGs in the sera in a dose-dependent
386 fashion, while no human IgGs were detected in the placebo group (Figure 7H - I). Human IgGs
387 were detected at three and up to 11 days post infection (Figure 7H - I).

388

389 **DISCUSSION**

390 This work describes a systematic screening of memory B cells from SARS-CoV-2 convalescent
391 patients to identify extremely potent mAbs against SARS-CoV-2 and their engineering to extend
392 half-life and eliminate the potential risk of ADE. The best antibody neutralized the authentic wild
393 type virus and emerging variants at pico molar concentration *in vitro* and showed prophylactic and
394 therapeutic efficacy in a SARS-CoV-2 hamsters model of infection when used at 0.25 and 4 mg/kg
395 respectively. The antibody described is a promising candidate for the development of a broadly
396 affordable tool for prevention and therapy of COVID-19.

397 In the search for potent antibodies, we found that approximately 10% of the total B cells against the
398 S-protein isolated produce neutralizing antibodies and these can be divided into 4 different groups
399 recognizing the S1-RBD, S1-domain, S2-domain and the S-protein trimer. Most potently
400 neutralizing antibodies are extremely rare and recognize the RBD, followed in potency by
401 antibodies recognizing the S1 domain, the trimeric structure and the S2 subunit. From these data
402 we can conclude that in COVID-19 convalescent patients most of the observed neutralization titers
403 are likely mediated by antibodies with medium-high neutralizing potency. Indeed, the extremely
404 potent antibodies and the antibodies against the S2 subunit are unlikely to contribute to the overall
405 neutralizing titers because they are respectively too rare and too poor neutralizers to be able to
406 make a difference. We and others found that the antibody repertoire of convalescent patients is
407 mostly germline-like. This may be a consequence of the loss of Bcl-6-expressing follicular helper T
408 cells and the loss of germinal centers in COVID-19 patients which may limit and constrain the B cell
409 affinity maturation (Kaneko et al., 2020). It will be therefore important to perform similar studies
410 following vaccination as it is likely that the repertoire of neutralizing antibodies induced by
411 vaccination may be different from the one described here.

412 Out of the 453 neutralizing antibodies that were tested and characterized, one antibody (J08)
413 showed extremely high neutralization potency against both the wild type SARS-CoV-2 virus
414 isolated in Wuhan and emerging variants containing the D614G, E484K and N501Y variants.
415 During the last few months several groups reported the identification, three-dimensional structure
416 and passive protection in animal models of neutralizing antibodies against SARS-CoV-2. Most of

417 these studies, with few exceptions, reported antibodies which require from 20 to several hundred
418 ng/mL to neutralize 50% of the virus *in vitro*. While these antibodies are potentially good for
419 therapy, they will require a high dosage which is associated with elevated cost of goods, low
420 production capacity and delivery by intravenous infusion.

421 The extremely potent mAb described in our study is likely to allow to use lower quantities of
422 antibodies to reach prophylactic and therapeutic efficacy and as a consequence decrease the cost
423 of goods and enable sustainable development and manufacturability. This solution may increase
424 the number of doses produced annually and therefore increase antibodies availability in high
425 income countries as well as low-and middle-income countries (LMICs). Therefore our antibodies
426 have the potential to meet the expectations of the call to action to expand access to monoclonal
427 antibody-based products, recently published by the Wellcome Trust, and supported by the WHO
428 and the Coalition for Epidemic Preparedness Innovations (CEPI) (Wellcome, 2020).

429 A potential issue associated with the use of human monoclonal antibodies against viral pathogens
430 is the potential selection of escape mutants. This is usually addressed by using a combination of
431 antibodies directed against non-overlapping epitopes. While this is an ultimate clear solution, it
432 increases the complexity of development, costs of production, drug availability and affordability. In
433 our case we believe that selection of escape mutants upon treatment with a single monoclonal
434 antibody may be quite difficult as the SARS-CoV-2 RNA-dependent polymerase possesses a
435 proofreading machinery (Romano et al., 2020) and the epitope recognized by the antibodies herein
436 described overlaps with the region necessary to bind the hACE2 receptor. In this regard, it took
437 more than 70 days of continuous co-culture of the virus in presence of the antibodies before we
438 were able to detect the first emergence of escape mutants of the wild-type SARS-CoV-2 (data not
439 shown).

440 Finally, a peculiar part of our approach consisted in depleting possible antibody Fc-mediated
441 functions of the antibodies to avoid the risk of ADE. While there is no evidence of ADE in SARS-
442 CoV-2, and most vaccines and mAbs tested so far seem to be safe, it is too early to make definitive
443 conclusions. In addition, two recently published reports suggested that we need to continue to
444 monitor the potential risk of ADE. The first report showed that severe SARS-CoV-2 patients are

445 characterized by an increased proinflammatory signature mediated by the Fc γ receptors triggered
446 by afucosylated IgG1 antibodies (Chakraborty et al., 2020). The second report described that one
447 antibody was associated with worse clinical outcomes when administered to hospitalized patients
448 requiring high flow oxygen or mechanical ventilation (Lilly, 2020). Therefore, we believe it is
449 important to develop and test antibodies where Fc-mediated functions have been eliminated in the
450 clinical practice. Since the Fc portion contributes significantly to the *in vivo* potency of the
451 antibodies (Schäfer et al., 2020), removing Fc-functions may be a problem for mAbs with low
452 neutralization potency because they may no longer be effective when tested in clinical settings, as
453 already described in other contexts (DiLillo et al., 2014). The extremely high potency shown by our
454 antibodies allowed us to remove Fc-functions while maintaining *in vivo* potency at minimal dosage.

455

456 **Limitations of the study**

457 While we believe that our antibodies are extremely potent when compared to most of those
458 described in literature, we acknowledge that in most cases direct comparison was not performed
459 and we rely on published data.

460 The second limitation of the study is that *in vitro* neutralization and *in vivo* protection in the SARS-
461 CoV-2 hamster model of infection cannot be fully predictive of the behavior of the same antibody in
462 humans and therefore the real benefit of described antibodies can only be assessed in clinical
463 studies.

464

Journal Pre-proof

465 **ACKNOWLEDGMENTS**

466 We wish to thank Fondazione Toscana Life Sciences in the persons of Dr. Fabrizio Landi and Dr.
467 Andrea Paolini and the whole Administration for their help and support. In particular we would like
468 to thank Mr. Francesco Senatore, Mrs. Laura Canavacci and Mrs. Cinzia Giordano for their support
469 in preparing all the documents needed for the ethical approval of the clinical studies carried out
470 within this project.

471 We wish to thank the National Institute for Infectious Diseases, IRCCS, Lazzaro Spallanzani Rome
472 (IT) and the Azienda Ospedaliera Universitaria Senese, Siena (IT), for providing blood samples
473 from Covid-19 convalescent donors under studies approved by local ethic committees. We also
474 wish to thank all the nursing staff who chose to cooperate for blood withdrawal and all the donors
475 who decided to participate in this study.

476 We would like to thank the whole GSK Vaccines Pre-clinical Evidence Generation and Assay -
477 Immunology function led by Dr. Oretta Finco for their availability and support as well as Mrs. Simona
478 Tavarini, Mrs. Chiara Sammiceli, Dr. Monia Bardelli, Dr. Michela Brazzoli, Dr. Elisabetta
479 Frigimelica, Dr. Erica Borgogni and Dr. Elisa Faenzi for sharing their expertise, extreme availability
480 and technical support. We would also like to thank Dr. Mariagrazia Pizza and Dr. Simone Pecetta
481 for initial insightful advice and discussions on this project.

482 We would like to thank Dr. Jason McLellan and his team for generously providing the SARS-CoV-2
483 S-protein stabilized in its prefusion conformation used in this study. Furthermore, we would like to
484 thank Dr. Daniel Wrapp and Dr. Nianshuang Wang for the precious information and suggestions.

485 The authors wish to thank Seromyx for their support in assessing the functionality of the antibodies
486 Fc-portion.

487 The authors would like to thank the University of Georgia Animal Resource staff, technicians, and
488 veterinarians for animal care as well as the staff of the University of Georgia AHRC BSL-3 facility
489 for providing biosafety and animal care. The following reagent was deposited by the Centers for
490 Disease Control and Prevention and obtained through BEI Resources, NIAID, NIH: SARS-Related
491 Coronavirus 2 Isolate USA-WA1/2020, NR-52281.

492 This work was funded by the European Research Council (ERC) advanced grant agreement
493 number 787552 (vAMRes).

494 This publication was supported by funds from the “Centro Regionale Medicina di Precisione” and
495 by all the people who answered the call to fight with us the battle against SARS-CoV-2 with their
496 kind donations on the platform ForFunding
497 (<https://www.forfunding.intesasanpaolo.com/DonationPlatform-ISP/nav/progetto/id/3380>).

498 This publication was supported by the European Virus Archive goes Global (EVAg) project, which
499 has received funding from the European Union’s Horizon 2020 research and innovation
500 programme under grant agreement No 653316.

501 This publication was supported by the COVID-2020-12371817 project, which has received funding
502 from the Italian Ministry of Health.

503 This work was funded, in part, by the University of Georgia (UGA) (UGA-001) and a contract by
504 Toscana Life Sciences Institute. In addition, TMR is supported by the Georgia Research Alliance
505 as an Eminent Scholar.

506 We wish to thank AchilleS Vaccines and the EU Malaria Fund for funding and managing the
507 development of the human monoclonal antibody for clinical studies.

508

509 **AUTHOR CONTRIBUTIONS**

510 EA, IP, PP, NM, EP, GP, AM, LB, MT, FV, AK, JB, LD, CDG, HJ, GS, JT, GO, CDS and DC
511 conceived, performed experiments and analyzed data. EN, CA, CC, FM, AE, MF enrolled patients
512 and isolated PBMCs. RR and EA wrote the manuscript. AW, EM, NT, TR, MRC, GI, LB, CS and
513 RR coordinated the project.

514

Journal Pre-proof

515 **DECLARATION OF INTERESTS**

516 Rino Rappuoli is an employee of GSK group of companies.

517 Emanuele Andreano, Anna Kabanova, Dario Cardamone, Concetta De Santi, Ida Paciello, Noemi
518 Manganaro, Elisa Pantano, Piero Pileri, Claudia Sala, Marco Troisi, Fabiola Vacca and Rino
519 Rappuoli are listed as inventors of full-length human monoclonal antibodies described in Italian
520 patent applications n. 102020000015754 filed on June 30th 2020 and 102020000018955 filed on
521 August 3rd 2020.

Journal Pre-proof

522 **FIGURE LEGENDS**523 **Figure 1. Workflow and timeline for SARS-CoV-2 neutralizing antibodies identification**

524 The overall scheme shows three different phases for the identification of SARS-CoV-2 neutralizing
525 antibodies (nAbs). Phase 1 consisted in the enrolment of Covid-19 patients (N=14) from which
526 PBMCs were isolated. Memory B cells were single cell sorted (N=4,277) and after 2 weeks of
527 incubation antibodies were screened for their binding specificity against the S-protein trimer and
528 S1/S2 domains. Once S-protein specific monoclonal antibodies were identified (N=1,731) phase 2
529 started. All specific mAbs were tested *in vitro* to evaluate their neutralization activity against the
530 authentic SARS-CoV-2 virus and 453 nAbs were identified. nAbs showing different binding profiles
531 on the S-protein surface were selected for further functional characterization and to identify
532 different neutralizing regions on the antigen. Phase 3 starts with the characterization of the heavy
533 and light chain sequences of selected mAbs (N=14) and the engineering of the Fc-portion of three
534 most promising candidates. These latter were also selected for structural analyses that allowed the
535 identification of the neutralizing epitopes on the S-protein. Finally, the most potent antibody was
536 tested for its prophylactic and therapeutic effect in a golden Syrian hamster model of SARS-CoV-2
537 infection.

538

539 **Figure 2. Identification of SARS-CoV-2 S-protein specific neutralizing antibodies (nAbs)**

540 (A) The graph shows supernatants tested for binding to the SARS-CoV-2 S-protein stabilized in its
541 prefusion conformation. Threshold of positivity has been set as two times the value of the blank
542 (dotted line). Red dots represent mAbs which bind to the S-protein while pink dots represent mAbs
543 which do not bind. (B) The bar graph shows the percentage of non-neutralizing (gray), partially
544 neutralizing (pale yellow) and neutralizing mAbs (dark red) identified per each donor. The total
545 number (N) of antibodies tested per individual is shown on top of each bar. (C) The graph shows
546 the neutralization potency of each nAb tested once expressed as recombinant full-length IgG1.
547 Dashed lines show different ranges of neutralization potency (500, 100 and 10 ng/mL). Dots were
548 colored based on their neutralization potency and were classified as weakly neutralizing (>500
549 ng/mL; pale orange), medium neutralizing (100 - 500 ng/mL; orange), highly neutralizing (10 - 100
550 ng/mL; dark orange) and extremely neutralizing (1 - 10 ng/mL; dark red). The total number (N) of

551 antibodies tested per individual is shown on top of each graph. A COVID-19 convalescent plasma
552 and an unrelated plasma were used as positive and negative control respectively in all the assays.

553

554 **Figure 3. Functional characterization of potent SARS-CoV-2 S-protein specific nAbs**

555 (A - B - C) Graphs show binding curves to the S-protein in its trimeric conformation, S1-domain and
556 S2-domain. Mean \pm SD of technical triplicates are shown. Dashed lines represent the threshold of
557 positivity; (D - F) Neutralization curves for selected antibodies were shown as percentage of viral
558 neutralization against the authentic SARS-CoV-2 wild type (D), D614G variant (E) and the
559 emerging variant B.1.1.7 (F). Data are representative of technical triplicates. A neutralizing COVID-
560 19 convalescent plasma and an unrelated plasma were used as positive and negative control
561 respectively. (G - I) Neutralization potency of fourteen selected antibodies against the authentic
562 SARS-CoV-2 wild type (G), D614G variant (H) and the emerging variant B.1.1.7 (I). Dashed lines
563 show different ranges of neutralization potency (500, 100 and 10 ng/mL). In all graphs selected
564 antibodies are shown in dark red, pink, gray and light blue based on their ability to recognize the
565 SARS-CoV-2 S1-RBD, S1-domain, S-protein trimer only and S2-domain respectively.

566

567 **Figure 4. Identification of four different sites of pathogen vulnerability on the S-protein surface**

568 (A) Representative cytometer peaks per each of the four antibody groups are shown. Positive
569 (beads conjugated with only primary labelled antibody) and negative (un-conjugated beads)
570 controls are shown as green and red peaks respectively. Competing and not-competing nAbs are
571 shown in blue and gray peaks respectively. (B) The heatmap shows the competition matrix
572 observed among the 14 nAbs tested. Threshold of competition was set at 50% of fluorescent signal
573 reduction. A speculative representation of the vulnerability sites is shown on the S-protein surface.

574

575 **Figure 5 Heavy and light chain analyses of selected nAbs**

576 (A - B) Bar graphs show the heavy and light chains usage for neutralizing antibodies against
577 SARS-CoV-2 in the public repertoire compared to the antibodies identified in this study. Our and
578 public antibodies are shown in dark and light colors respectively. (C - D) The heavy and light chain
579 percentage of identity to the inferred germline and amino acidic CDR3 length are shown as violin

580 and distribution plot respectively. (E) The heatmap shows the frequency of heavy and light chain
 581 pairing for SARS-CoV-2 neutralizing human monoclonal antibodies already published. The number
 582 within the heatmap cells represent the amount of nAbs described in this manuscript showing
 583 already published (colored cells) or novel heavy and light chain rearrangements (blank cells).

584

585 **Figure 6. EM epitope mapping of RBD mAbs**

586 (A) Negative stain for J08, I14 and F05 in complex with the S-protein. 200 nm scale bar is shown;
 587 (B) Figures show the binding of J08 (blue), I14 (green) and F05 (red) to the SARS-CoV-2 S-protein
 588 RBD.

589

590 **Figure 7. Prophylactic and therapeutic efficacy of J08-MUT in the golden Syrian hamster model of**
 591 **SARS-CoV-2 infection**

592 (A) Schematic representation and timelines of prophylactic and therapeutic studies performed in
 593 golden Syrian hamster. (B) The figure shows the prophylactic impact of J08-MUT at three different
 594 concentrations (4 - 1 - 0.25 mg/kg) on body weight loss change (C). The figure shows the
 595 therapeutic impact of J08-MUT at 4 mg/kg on body weight loss change. (D - F) The figures show
 596 the lung viral titer at day 3 (D) and the detection of human antibodies in hamster sera at day 3 (E)
 597 and day 8 (F) in the prophylactic study. (G - I) The figures show the lung viral titer at day 3 (G) and
 598 the detection of human antibodies in hamster sera at day 3 (H) and day 12 (I) in the therapeutic
 599 study. Statistically differences were calculated with two-way analysis of variance (ANOVA) for body
 600 weight change and with a nonparametric Mann-Whitney t-test for the lung viral titer. Significances
 601 are shown as * ($p \leq 0.05$), ** ($p \leq 0.01$), *** ($p \leq 0.001$) and **** ($p \leq 0.0001$).

602

603 **Figure S1. Gating strategy for single cell sorting and monoclonal antibodies screening for S-protein**
 604 **S1 + S2 subunits binding and neutralization of binding (NoB) activity, related to Figure 2**

605 (A) Starting from top left to the right panel, the gating strategy shows: Live/Dead; Morphology;
 606 $CD19^+$ B cells; $CD19^+CD27^+IgD^-$; $CD19^+CD27^+IgD^-IgM^-$; $CD19^+CD27^+IgD^-IgM^-S\text{-protein}^+$ B cells.
 607 (B) The graph shows supernatants tested for binding to the SARS-CoV-2 S-protein S1 + S2
 608 subunits. Threshold of positivity has been set as two times the value of the blank (dotted line).

609 Darker dots represent mAbs which bind to the S1 + S2 while light yellow dots represent mAbs
610 which do not bind. (B) The graph shows supernatants tested by NoB assay. Threshold of positivity
611 has been set as 50% of binding neutralization (dotted line). Dark blue dots represent mAbs able to
612 neutralize the binding between SARS-CoV-2 and receptors on Vero E6 cells, while light blue dots
613 represent non-neutralizing mAbs.

614

615 **Figure S2. Characterization and distribution of SARS-CoV-2 S-protein specific nAbs, related to**

616 **Figure 2**

617 (A) The bar graph shows the distribution of nAbs binding to different S-protein domains. In dark
618 red, light blue and gray are shown antibodies binding to the S1-domain, S2-domain and S-protein
619 trimer respectively. The total number (N) of antibodies tested per individual is shown on top of each
620 bar. (B) The bar graph shows the distribution of nAbs with different neutralization potencies. nAbs
621 were classified as weakly neutralizing (>500 ng/mL; pale orange), medium neutralizing (100 - 500
622 ng/mL; orange), highly neutralizing (10 - 100 ng/mL; dark orange) and extremely neutralizing (1 -
623 10 ng/mL; dark red). The total number (N) of antibodies tested per individual is shown on top of
624 each bar.

625

626 **Figure S3. Binding to S-protein receptor binding domain (RBD) and NoB activity of S1-RBD**
627 **antibodies, related to Figure 3**

628 (A) Histograms show the ability of selected antibodies to bind the S-protein RBD. Gray histograms
629 represent the negative control while colored histograms show tested antibodies. Percentage of
630 positive and negative populations are denoted on each graph. (B) Neutralization of binding (NoB)
631 curves for S1-RBD specific antibodies are shown as percentage of reduction of signal emitted by a
632 fluorescently labeled S-protein incubated with Vero E6 cells. Mean \pm SD of technical duplicates are
633 shown. Dashed lines represent the threshold of positivity; A neutralizing COVID-19 convalescent
634 plasma and an unrelated plasma were used as positive and negative control respectively.

635

636 **Figure S4. Binding kinetics of SARS-CoV-2 nAbs to the S-protein antigen, related to Figure 3**

637 Representative binding curves of selected antibodies to SARS-CoV-2 S-protein trimer. Different
638 curve colors define the spike concentration used in the experiment. Kon, Koff and KD are denoted
639 on each graph.

640

641 **Fig S5. Neutralization activity of selected nAbs against SARS-CoV-2, SARS-CoV and MERS-CoV**
642 **pseudotypes, related to Figure 3**

643 (A - D) Graphs show the neutralizing activities of 14 selected nAbs with different SARS-CoV-2 S-
644 protein binding profiles against SARS-CoV-2, SARS-CoV-2 D614G, SARS-CoV and MERS-CoV
645 pseudotypes respectively. Dashed lines represent the threshold of positivity. Mean \pm SD of
646 technical duplicates are shown. In all graphs selected antibodies are shown in dark red, pink, gray
647 and light blue based on their ability to recognize the SARS-CoV-2 S1-RBD, S1-domain, S-protein
648 trimer only and S2-domain respectively.

649

650 **Fig S6. Characterization of Fc-engineered candidate nAbs, related to Figure 7**

651 (A) the graph shows binding curves of J08, I14 and F05 MUT and WT to the Fc γ R2A. (B - C)
652 graphs show binding curves of J08, I14 and F05 MUT and WT to the FcRn at pH 6.2 (B) and 7.4
653 (C). (D - E) Graphs show the ADNP and ADNK induced by J08, I14 and F05 MUT and WT
654 versions; all the experiments were run as technical duplicates. In every experiment a control
655 antibody (CR3022) and an unrelated protein were used as positive and negative control
656 respectively. (F - G - H) Graphs show binding curves to the S-protein in its trimeric conformation,
657 S1-domain and S2-domain. Mean of technical triplicates are shown. (I - J - K) Neutralization curves
658 against the authentic SARS-CoV-2 wild type, the D614G variant and the B.1.1.7 emerging variant
659 for J08-MUT, I14-MUT and F05-MUT shown in blue, green and red respectively. Data are
660 representative of technical triplicates.

661

662 **Fig S7. Autoreactivity assessment of selected SARS-CoV-2 candidate nAbs, related to Figure 7**

663 (A) Schematic representation of the indirect immunofluorescent assay for the screening of
664 autoreactive nAb. (B) Single figures show the fluorescent signal detected per each sample tested in
665 this assay. Positive and negative controls were used at three different dilutions (1:1, 1:10 and

666 1:100). Three candidate nAbs were incubated on HEp-2 cells at a concentration of 100 µg/mL.
667 Representative pictures of the scoring system are shown. Autoreactive samples are highlighted in
668 pink.

Journal Pre-proof

669 STAR METHODS

670 KEY RESOURCES TABLE

REAGENT or RESOURCE	SOURCE	IDENTIFIER
Antibodies and Fluorophores		
CD19 V421	BD Biosciences	Cat#562440
IgM PerCP-Cy5.5	BD Biosciences	Cat#561285
CD27 PE	BD Biosciences	Cat#340425
IgD-A700	BD Biosciences	Cat#561302
CD3 PE-Cy7	BioLegend	Cat#300420
CD14 PE-Cy7	BioLegend	Cat#301814
Streptavidin-PE	Thermo Fisher	Cat#12-4317-87
Goat Anti-Human IgA-UNLB	Southern Biotech	Cat#2050-01
Goat Anti-Human IgA-Alkaline Phosphatase	Southern Biotech	Cat#2050-04
Goat Anti-Human IgG-UNLB	Southern Biotech	Cat#2040-01
Bacterial and Virus Strains		
SARS-CoV-2 wild type	EVAg	GenBank: MT066156.1
SARS-CoV-2 D614G	EVAg	GenBank: MT527178.1
SARS-CoV-2 B.1.1.7	INMI	GISAID accession number: EPI_ISL_736997
Biological Samples		
PBMCs and IgGs of donor PT-004	This paper	N/A
PBMCs and IgGs of donor PT-005	This paper	N/A
PBMCs and IgGs of donor PT-006	This paper	N/A
PBMCs and IgGs of donor PT-008	This paper	N/A
PBMCs and IgGs of donor PT-009	This paper	N/A
PBMCs and IgGs of donor PT-010	This paper	N/A
PBMCs and IgGs of donor PT-012	This paper	N/A
PBMCs and IgGs of donor PT-014	This paper	N/A
PBMCs and IgGs of donor PT-041	This paper	N/A
PBMCs and IgGs of donor PT-100	This paper	N/A
PBMCs and IgGs of donor PT-101	This paper	N/A
PBMCs and IgGs of donor PT-102	This paper	N/A
PBMCs and IgGs of donor PT-103	This paper	N/A
PBMCs and IgGs of donor PT-188	This paper	N/A
Chemicals, Peptides, and Recombinant Proteins		
Fetal Bovine Serum (FBS) Hyclone	Sigma-Aldrich	Cat#D2650
DMSO	Sigma-Aldrich	Cat#D2650

RNaseOUT Recombinant Ribonuclease Inhibitor	Thermo Fisher	Cat#10777-019
SuperScript IV Reverse Transcriptase	Thermo Fisher	Cat#18091200
DEPC-Treated water	Thermo Fisher	Cat#AM9916
dNTP Set (100 mM)	Thermo Fisher	Cat#10297018
MgCl ₂ Magnesium Chloride 25mM	Thermo Fisher	Cat#AB0359
Kapa Long Range Polymerase	Sigma-Aldrich	Cat#KK3005
NEBuilder® HiFi DNA Assembly Master Mix	New England BioLabs	Cat#E2621X
Q5® High-Fidelity DNA Polymerases	New England BioLabs	Cat#M0491L
Expi293™ Expression Medium	Thermo Fisher	Cat#A1435101
ExpiFectamine™ 293 Transfection Kit	Thermo Fisher	Cat#A14524
Ultra Pure Bovine serum albumin (BSA)	Thermo Fisher	Cat#AM2618
DMEM high Glucose	Thermo Fisher	Cat#11965092
Ficoll-Paque™ PREMIUM	Sigma-Aldrich	Cat#GE17-5442-03
MycoZap Plus-PR	Lonza	Cat#VZA2022
IMDM with GlutaMAX	Thermo Fisher	Cat# 31980048
Benzonase Nuclease	Sigma-Aldrich	Cat#70664-3
IL-2 Recombinant Human Protein	Thermo Fisher	Cat#PHC0023
IL-21 Recombinant Human Protein	Thermo Fisher	Cat#PHC0211
Strep-Tactin DY488	IBA lifesciences	Cat#2-1562-050
Slide-A-Lyzer™ Dialysis Cassettes	Thermo Fisher	Cat#66003
HiTrap Protein G HP column	Cytiva	Cat#17040503
HisTrap FF Crude column	Cytiva	Cat#17528601
SARS Coronavirus Spike Glycoprotein (S1)	The Native Antigen Company	Cat#REC31809
SARS Coronavirus Spike Glycoprotein (S2)	The Native Antigen Company	Cat#REC31807
Tween-20	VWR	Cat#A4974.0250
SARS Coronavirus Spike Glycoprotein (S1)	The Native Antigen Company	Cat#REC31806-500
SARS Coronavirus Spike Glycoprotein (S2)	The Native Antigen Company	Cat#REC31807-500
Alkaline Phosphatase Yellow (pNPP) Liquid Substrate System	Sigma-Aldrich	Cat#P7998
Goat Anti-Human IgG-UNLB	SouthernBiotech	Cat#2040-01
Critical Commercial Assays		
NOVA Lite Hep-2 ANA Kit	Inova Diagnostics / Werfen	Cat#066708100
ELISA Starter Accessory Kit	Bethyl Laboratories	Cat#E101
APEX Alexa Fluor 647 Antibody Labeling Kit	Thermo Fisher	Cat#A10475
Pierce BCA Protein Assay Kit	Thermo Fisher	Cat#23227
Deposited Data		
Cloned and tested SARS-CoV-2-neutralizing antibodies	This paper	Patent Application

Experimental Models: Cell Lines

VERO E6 cell line	ATCC	Cat#CRL-1586
Expi293F™ cells	Thermo Fisher	Cat#A14527
3T3-msCD40L Cells	NIH AIDS Reagent Program	Cat#12535

Oligonucleotides

Single cell PCR Primer	This paper	N/A
Random Hexamer Primer	Thermo Fisher	Cat#SO142
TAP forward primer (TTAGGCACCCCAGGCTTTAC)	This paper	N/A
TAP forward primer (AGATGGTTCTTTCCGCCTCA)	This paper	N/A

Recombinant DNA

Human antibody expression vectors (IgG1, Igl, Igk)	(Tiller et al., 2008)	N/A
Plasmid encoding SARS-CoV-2 S ectodomain (amino acids 1-1208 of SARS-CoV-2 S; GenBank: MN908947)	(Wrapp et al., 2020)	N/A
Plasmid encoding SARS-CoV-2 RBD (amino acids 319 - 591 of SARS-CoV-2 S; GenBank: MN908947)	Jason McLellan Lab	N/A
pCDNA3.1+-SARS-CoV-2 Spike from Wuhan-Hu-1 isolate (Genbank MN908947.3) codon optimised	This paper	pCDNA-S2
pCAGGS-SARS-CoV-2 Spike from Wuhan-Hu-1 isolate (Genbank MN908947.3) encoding D614G mutation and codon optimised	This paper	pCAGGS-S2 D614G
pCAGGS-SARS1 Spike protein codon optimised	(Carnell et al., 2017)	pCAGGS-S1
pCAGGS-MERS Spike protein codon optimised	(Grehan et al., 2015)	pCAGGS-MERS
pCSFLW Firefly luciferase encoding plasmid	(Carnell et al., 2015)	pCSFLW
p8.91 HIV Gag/Pol-encoding plasmid	(Carnell et al., 2015)	p8.91

Software and Algorithms

Prism 8	GraphPad	https://www.graphpad.com/
FlowJo 10.5.3	FlowJo, LLC	https://www.flowjo.com
FastQC	Babraham Institute	https://www.bioinformatics.babraham.ac.uk/projects/fastqc/
MultiQC 1.9	MultiQC	https://multiqc.info/
Trimmomatic 0.39	USADELLAB	http://www.usadellab.org/c

		ms/?page=trimmomatic
MiXCR	MI Lanoratory	https://mixcr.readthedocs.io/en/master/index.html
NumPy	NumPy	https://numpy.org/
Python 3.7.4	Python Software Foundation	https://www.python.org/
Other		
BD FACS Aria III Cell Sorter	BD Biosciences	https://www.bdbiosciences.com
BD FACS Canto II	BD Biosciences	https://www.bdbiosciences.com
Leica DMI-microscope	Leica Biosystem	https://www.leica-microsystems.com
LUNA-II Automated Cell Counter	Logo Biosystems	https://logosbio.com
Qubit Fluorometric Quantification	Thermo Fisher	https://www.thermofisher.com
ÄKTA go	Cytiva Lifesciences	https://www.cytivalifesciences.com
GloMax Luminometer	Promega	https://ita.promega.com
Varioskan LUX multimode microplate reader	Thermo Fisher	https://www.thermofisher.com

671

672 RESOURCE AVAILABILITY**673 Lead Contact**

674 Further information and requests for resources and reagents should be directed to and will be
675 fulfilled by the Lead Contact, Rino Rappuoli (rino.r.rappuoli@gsk.com).

676

677 Materials Availability

678 Reasonable amounts of antibodies will be made available by the Lead Contact upon request under
679 a Material Transfer Agreement (MTA) for non-commercial usage.

680

681 Data and Code Availability

682 Nucleotide and amino acidic sequences of all SARS-CoV-2-neutralizing antibodies were deposited
683 in the Italian patent applications n. 102020000015754 filed on June 30th 2020 and
684 102020000018955 filed on August 3rd 2020. Nucleotide sequences of all SARS-CoV-2-neutralizing
685 antibodies were deposited at GenBank.

686

687 EXPERIMENTAL MODELS AND SUBJECT DETAILS**688 Enrollment of SARS-COV-2 convalescent donors and human sample collection**

689 This work results from a collaboration with the National Institute for Infectious Diseases, IRCCS -
690 Lazzaro Spallanzani Rome (IT) and Azienda Ospedaliera Universitaria Senese, Siena (IT) that
691 provided samples from SARS-CoV-2 convalescent donors, of both sexes, who gave their written
692 consent. The study was approved by local ethics committees (Parere 18_2020 in Rome and Parere
693 17065 in Siena) and conducted according to good clinical practice in accordance with the
694 declaration of Helsinki (European Council 2001, US Code of Federal Regulations, ICH 1997). This
695 study was unblinded and not randomized.

696

697 **METHOD DETAILS**698 **Single cell sorting of SARS-CoV-2 S-protein⁺ memory B cells from COVID-19 convalescent donors**

699 Blood samples were screened for SARS-CoV-2 RNA and for antibodies against HIV, HBV and
700 HCV. Peripheral blood mononuclear cells (PBMCs) were isolated from heparin-treated whole blood
701 by density gradient centrifugation (Ficoll-Paque™ PREMIUM, Sigma-Aldrich). After separation,
702 PBMC were stained with Live/Dead Fixable Aqua (Invitrogen; Thermo Scientific) in 100 µL final
703 volume diluted 1:500 at room temperature RT. After 20 min incubation cells were washed with PBS
704 and unspecific bindings were saturated with 50 µL of 20% normal rabbit serum (Life technologies)
705 in PBS . Following 20 min incubation at 4°C cells were washed with PBS and stained with SARS-
706 CoV-2 S-protein labeled with Strep-Tactin®XT DY-488 (iba-lifesciences cat# 2-1562-050) for 30
707 min at 4°C. After incubation the following staining mix was used CD19 V421 (BD cat# 562440), IgM
708 PerCP-Cy5.5 (BD cat# 561285), CD27 PE (BD cat# 340425), IgD-A700 (BD cat# 561302), CD3
709 PE-Cy7 (BioLegend cat# 300420), CD14 PE-Cy7 (BioLegend cat# 301814), CD56 PE-Cy7
710 (BioLegend cat# 318318) and cells were incubated at 4°C for additional 30 min. Stained MBCs
711 were single cell-sorted with a BD FACS Aria III (BD Biosciences) into 384-well plates containing
712 3T3-CD40L feeder cells and were incubated with IL-2 and IL-21 for 14 days as previously
713 described (Huang et al., 2013).

714

715 **Expression and purification of SARS-CoV-2 S-protein prefusion trimer and receptor binding domain**

716 Plasmid encoding SARS-CoV-2 S-2P construct (Wrapp et al., 2020) and S-protein RBD
717 (generously provided by Jason S. McLellan) were transiently transfected at 1 µg/mL culture into
718 Expi293F™ cells (Thermo Fisher) using ExpiFectamine™ 293 Reagent. Cells were grown for six
719 days at 37 °C with 8% CO₂ shaking 125 rpm according to the manufacturer's protocol (Thermo
720 Fisher); ExpiFectamine™ 293 Transfection Enhancers 1 and 2 were added 16 to 18 hours post-
721 transfection to boost transfection, cell viability, and protein expression. Cell cultures were
722 harvested three and six days after transfection. Cells were separated from the medium by
723 centrifugation (1,100 g for 10 min at 24°C). Collected supernatants were then pooled and clarified
724 by centrifugation (3,000 g for 15 min at 4°C) followed by filtration through a 0.45 µm filter.

725 Chromatography was conducted at room temperature using the ÄKTA go purification system from
726 GE Healthcare Life Sciences. Expressed proteins were purified by using an immobilized metal
727 affinity chromatography (FF Crude) followed by dialysis into final buffer. Specifically, the filtrated
728 culture supernatant was purified with a 5 mL HisTrap FF Crude column (GE Healthcare Life
729 Sciences) previously equilibrated in Buffer A (20 mM NaH₂PO₄, 500 mM NaCl + 30 mM imidazol
730 pH 7.4).

731 The flow rate for all steps of the HisTrap FF Crude column was 5 mL/min. The culture supernatant
732 of spike and RBD cell culture was applied to a single 5 mL HisTrap FF Crude column. The column
733 was washed in Buffer A for 4 column volumes (CV) with the all 4 CV collected as the column wash.
734 Recombinant proteins were eluted from the column applying a first step elution of 4 CV of 50%
735 Buffer B (20 mM NaH₂PO₄, 500 mM NaCl + 500 mM imidazol pH 7.4) and a second step elution of
736 2 CV of 100% Buffer B. Elution steps were collected in 1 fractions of 1 mL each. Eluted fractions
737 were analyzed by SDS-PAGE and appropriate fractions containing recombinant proteins were
738 pooled. Final pools were dialyzed against phosphate buffered saline (PBS) pH 7.4 using Slide-A-
739 Lyzer™ G2 Dialysis Cassette 3.5K (Thermo Scientific) overnight at 4°C. The dialysis buffer used
740 was at least 200 times the volume of the sample.

741 The final protein concentration was determined by measuring the A520 using the Pierce™ BCA
742 protein assay kit (Thermo Scientific™). Final protein was dispensed in aliquots of 0.5 ml each and
743 stored at -80°C.

744

745 **ELISA assay with S1 and S2 subunits of SARS-CoV-2 S-protein**

746 The presence of S1- and S2-binding antibodies in culture supernatants of monoclonal S-protein-
747 specific memory B cells was assessed by means of an ELISA implemented with the use of a
748 commercial kit (ELISA Starter Accessory Kit, Catalogue No. E101; Bethyl Laboratories). Briefly,
749 384-well flat-bottom microtiter plates (384 well plates, Microplate Clear, Greiner Bio-one) were
750 coated with 25 µL/well of antigen (1:1 mix of S1 and S2 subunits, 1 µg/mL each; The Native
751 Antigen Company, Oxford, United Kingdom) diluted in coating buffer (0.05 M carbonate-
752 bicarbonate solution, pH 9.6), and incubated overnight at 4°C. The plates were then washed three

753 times with 100 μL /well washing buffer (50 mM Tris Buffered Saline (TBS) pH 8.0, 0.05% Tween-20)
754 and saturated with 50 μL /well blocking buffer containing Bovine Serum Albumin (BSA) (50 mM TBS
755 pH 8.0, 1% BSA, 0.05% Tween-20) for 1 hour (h) at 37°C. After further washing, samples diluted
756 1:5 in blocking buffer were added to the plate. Blocking buffer was used as a blank. After an
757 incubation of 1 h at 37°C, plates were washed and incubated with 25 μL /well secondary antibody
758 (horseradish peroxidase (HRP)-conjugated goat anti-human IgG-Fc Fragment polyclonal antibody,
759 diluted 1:10,000 in blocking buffer, Catalogue No. A80-104P; (Bethyl Laboratories) for 1 h at 37°C.
760 After three washes, 25 μL /well TMB One Component HRP Microwell Substrate (Bethyl
761 Laboratories) was added and incubated 10-15 minutes at RT in the dark. Color development was
762 terminated by addition of 25 μL /well 0.2 M H_2SO_4 . Absorbance was measured at 450 nm in a
763 Varioskan Lux microplate reader (Thermo Fisher Scientific). Plasma from COVID-19 convalescent
764 donors (Andreano et al., 2020) and unrelated plasma were used as positive and negative control
765 respectively. The threshold for sample positivity was set at twice the optical density (OD) of the
766 blank.

767

768 **ELISA assay with SARS-CoV-2 S-protein prefusion trimer and S1 - S2 subunits**

769 ELISA assay was used to detect SARS-CoV-2 S-protein specific mAbs and to screen plasma from
770 SARS-CoV-2 convalescent donors. 384-well plates (384 well plates, microplate clear; Greiner Bio-
771 one) were coated with 3 $\mu\text{g}/\text{mL}$ of streptavidin (Thermo Fisher) diluted in coating buffer (0.05 M
772 carbonate-bicarbonate solution, pH 9.6) and incubated at RT overnight. Plates were then coated
773 with SARS-CoV-2 S-protein, S1 or S2 domains at 3 $\mu\text{g}/\text{mL}$ and incubated for 1h at RT. 50 μL /well
774 of saturation buffer (PBS/BSA 1%) was used to saturate unspecific binding and plates were
775 incubated at 37°C for 1h without CO_2 . For the first round of screening, supernatants were diluted
776 1:5 in PBS/BSA 1%/Tween20 0.05% in 25 μL /well final volume and incubated for 1h at 37°C
777 without CO_2 . For purified antibodies, and to assess EC_{50} , mAbs were tested at a starting
778 concentration of 5 $\mu\text{g}/\text{mL}$ and diluted step 1:2 in PBS/BSA 1%/Tween20 0.05% in 25 μL /well final
779 volume for 1h at 37°C without CO_2 . 25 μL /well of alkaline phosphatase-conjugated goat anti-human
780 IgG (Sigma-Aldrich) and IgA (Southern Biotech) were used as secondary antibodies. Wells were

781 washed three times between each step with PBS/BSA 1%/Tween20 0.05%. pNPP (p-nitrophenyl
782 phosphate) (Sigma-Aldrich) was used as soluble substrate to detect SARS-CoV-2 S-protein, S1 or
783 S2 specific mAbs and the final reaction was measured by using the Varioskan Lux Reader (Thermo
784 Fisher Scientific) at a wavelength of 405 nm. Plasma from COVID-19 convalescent donors
785 (Andreano et al., 2020) and unrelated plasma were used as positive and negative control
786 respectively. Samples were considered as positive if OD at 405 nm (OD_{405}) was twice the blank.

787

788 **SARS-CoV-2 virus and cell infection**

789 African green monkey kidney cell line Vero E6 cells (American Type Culture Collection [ATCC]
790 #CRL-1586) were cultured in Dulbecco's Modified Eagle's Medium (DMEM) - high glucose
791 (Euroclone, Pero, Italy) supplemented with 2 mM L- Glutamine (Lonza, Milano, Italy), penicillin (100
792 U/mL) - streptomycin (100 μ g/mL) mixture (Lonza, Milano, Italy) and 10% Foetal Bovine Serum
793 (FBS) (Euroclone, Pero, Italy). Cells were maintained at 37°C, in a 5% CO₂ humidified environment
794 and passaged every 3-4 days.

795 Wild type SARS-CoV-2 (SARS-CoV-2/INMI1-Isolate/2020/Italy: MT066156), D614G (SARS-CoV-
796 2/human/ITA/INMI4/2020, clade GR, D614G (S): MT527178) and B.1.1.7 (INMI-118 GISAID
797 accession number EPI_ISL_736997) viruses were purchased from the European Virus Archive
798 goes Global (EVAg, Spallanzani Institute, Rome) or received from the Spallanzani Institute, Rome.
799 For virus propagation, sub-confluent Vero E6 cell monolayers were prepared in T175 flasks
800 (Sarstedt) containing supplemented D-MEM high glucose medium. For titration and neutralization
801 tests of SARS-CoV-2, Vero E6 were seeded in 96-well plates (Sarstedt) at a density of 1.5×10^4
802 cells/well the day before the assay.

803

804 **Neutralization of Binding (NoB) Assay**

805 To study the binding of the SARS-CoV-2 S-protein to cell-surface receptor(s) we developed an
806 assay to assess recombinant S-protein specific binding to target cells and neutralization thereof. To
807 this aim the stabilized S-protein was coupled to Streptavidin-PE (eBioscience # 12-4317-87,
808 Thermo Fisher) for 1h at RT and then incubated with Vero E6 cells. Binding was assessed by flow

809 cytometry. The stabilized S-protein bound Vero E6 cells with high affinity (data not shown). To
810 assess the content of neutralizing antibodies in sera or in B-cell culture supernatants, two
811 microliters of SARS-CoV-2 Spike-Streptavidin-PE at 5 - 10 $\mu\text{g}/\text{mL}$ in PBS-5%FCS were mixed with
812 two microliters of various dilutions of sera or B-cell culture supernatants in U bottom 96-well plates.
813 After incubation at 37°C for 1 hr, 30×10^3 Vero E6 cells suspended in two microliters of PBS 5%
814 FCS were added and incubated for additional 45 min at 4°C. Non-bound protein and antibodies
815 were removed and cell-bound PE-fluorescence was analyzed with a FACS Canto II flow cytometer
816 (Becton Dickinson). Data were analyzed using the FlowJo data analysis software package
817 (TreeStar, USA). The specific neutralization was calculated as follows: $\text{NoB} (\%) = 1 - (\text{Sample MFI}$
818 $\text{value} - \text{background MFI value}) / (\text{Negative Control MFI value} - \text{background MFI value})$. Plasma
819 from COVID-19 convalescent donors (Andreano et al., 2020) and unrelated plasma were used as
820 positive and negative control respectively.

821

822 **Single cell RT-PCR and Ig gene amplification**

823 From the original 384-well sorting plate, 5 μL of cell lysate was used to perform RT-PCR. Total
824 RNA from single cells was reverse transcribed in 25 μL of reaction volume composed by 1 μL of
825 random hexamer primers (50 ng/ μL), 1 μL of dNTP-Mix (10 mM), 2 μL 0.1 M DTT, 40 U/ μL RNase
826 OUT, MgCl_2 (25 mM), 5x FS buffer and Superscript IV reverse transcriptase (Invitrogen). Final
827 volume was reached by adding nuclease-free water (DEPC). Reverse transcription (RT) reaction
828 was performed at 42°C/10', 25°C/10', 50°C/60' and 94°/5'. Heavy (VH) and light (VL) chain
829 amplicons were obtained via two rounds of PCR. All PCR reactions were performed in a nuclease-
830 free water (DEPC) in a total volume of 25 $\mu\text{L}/\text{well}$. Briefly, 4 μL of cDNA were used for the first
831 round of PCR (PCRI). PCRI-master mix contained 10 μM of VH and 10 μM VL primer-mix ,10mM
832 dNTP mix, 0.125 μL of Kapa Long Range Polymerase (Sigma), 1.5 μL MgCl_2 and 5 μL of 5x Kapa
833 Long Range Buffer. PCRI reaction was performed at 95°/3', 5 cycles at 95°C/30", 57°C/30",
834 72°C/30" and 30 cycles at 95°C/30", 60°C/30", 72°C/30" and a final extension of 72°/2'. All nested
835 PCR reactions (PCRII) were performed using 3.5 μL of unpurified PCRI product using the same
836 cycle conditions. PCRII products were then purified by Millipore MultiScreen® PCR μ 96 plate

837 according to manufacture instructions. Samples were eluted with 30 μ L nuclease-free water
838 (DEPC) into 96-well plates and quantify by.

839

840 **Cloning of variable region genes and recombinant antibody expression in transcriptionally active** 841 **PCR**

842 Vector digestions were carried out with the respective restriction enzymes AgeI, Sall and Xho as
843 previously described (Tiller et al., 2008, Wardemann and Busse, 2019). Briefly, 75 ng of IgH, Ig λ
844 and Igk purified PCRII products were ligated by using the Gibson Assembly NEB into 25 ng of
845 respective human Igy1, Igk and Ig λ expression vectors. The reaction was performed into 5 μ L of
846 total volume. Ligation product was 10-fold diluted in nuclease-free water (DEPC) and used as
847 template for transcriptionally active PCR (TAP) reaction which allowed the direct use of linear DNA
848 fragments for *in vitro* expression. The entire process consists of one PCR amplification step, using
849 primers to attach functional promoter (human CMV) and terminator sequences (SV40) onto the
850 fragment PCRII products. TAP reaction was performed in a total volume of 25 μ L using 5 μ L of Q5
851 polymerase (NEB), 5 μ L of GC Enhancer (NEB), 5 μ L of 5X buffer, 10 mM dNTPs, 0.125 μ L of
852 forward/reverse primers and 3 μ L of ligation product. TAP reaction was performed by using the
853 following cycles: 98°/2', 35 cycles 98°/10", 61°/20", 72°/1' and 72°/5' as final extension step. TAP
854 products were purified under the same PCRII conditions, quantified by Qubit Fluorometric
855 Quantitation assay (Invitrogen) and used for transient transfection in Expi293F cell line using
856 manufacturing instructions.

857

858 **Flask expression and purification of human monoclonal antibodies**

859 Expi293F™ cells (Thermo Fisher) were transiently transfected with plasmids carrying the antibody
860 heavy chain and the light chains with a 1:2 ratio. Cells were grown for six days at 37 °C with 8%
861 CO₂ shaking at 125 rpm according to the manufacturer's protocol (Thermo Fisher);
862 ExpiFectamine™ 293 transfection enhancers 1 and 2 were added 16 to 18 hours post-transfection
863 to boost cell viability and protein expression. Cell cultures were harvested three and six days after
864 transfection. Cells were separated from the medium by centrifugation (1,100 g for 10 min at 24°C).

865 Supernatants collected were then pooled and clarified by centrifugation (3000 g for 15 min, 4°C)
866 followed by filtration through a 0.45 µm filter. Chromatography was conducted at room temperature
867 using the ÄKTA go purification system from GE Healthcare Life Sciences. Affinity chromatography
868 was used to purify expressed monoclonal antibodies using an immobilized protein G column able
869 to bind to Fc region. Specifically, filtrated culture supernatants were purified with a 1 mL HiTrap
870 Protein G HP column (GE Healthcare Life Sciences) previously equilibrated in Buffer A (0.02 M
871 NaH₂PO₄ pH 7). The flow rate for all steps of the HiTrap Protein G HP column was 1 mL/min. The
872 culture supernatant for every monoclonal antibody cell culture was applied to a single 1 mL HiTrap
873 Protein G HP column. The column was equilibrated in Buffer A for at least 6 column volumes (CV)
874 which was collected as column wash. Each monoclonal antibody was eluted from the column
875 applying a step elution of 6 CV of Buffer B (0.1 M glycine-HCl, pH 2.7). Elution steps were collected
876 in 1 fractions of 1 mL each. Eluted fractions were analyzed by non-reducing SDS-PAGE and
877 fractions showing the presence of IgG were pooled together. Final pools was dialyzed in PBS
878 buffer pH 7.4 using Slide-A-Lyzer™ G2 Dialysis Cassette 3.5K (Thermo Scientific) overnight at 4°C.
879 The dialysis buffer used was at least 200 times the volume of the sample. For each antibody
880 purified the concentration was determined by measuring the A520 using Pierce™ BCA Protein
881 Assay Kit (Thermo Scientific). All the purified antibodies were aliquoted and stored at -80°C.

882

883 **Viral propagation and titration**

884 The SARS-CoV-2 virus was propagated in Vero E6 cells cultured in DMEM high Glucose
885 supplemented with 2% FBS, 100 U/mL penicillin, 100 µg/mL streptomycin. Cells were seeded at a
886 density of 1x10⁶ cells/mL in T175 flasks and incubated at 37°C, 5% CO₂ for 18 - 20 hours. The sub-
887 confluent cell monolayer was then washed twice with sterile Dulbecco's PBS (DPBS). Cells were
888 inoculated with 3,5 mL of the virus properly diluted in DMEM 2% FBS at a multiplicity of infection
889 (MOI) of 0.001, and incubated for 1h at 37°C in a humidified environment with 5% CO₂. At the end
890 of the incubation, 50 mL of DMEM 2% FBS were added to the flasks. The infected cultures were
891 incubated at 37°C, 5% CO₂ and monitored daily until approximately 80-90% of the cells exhibited
892 cytopathic effect (CPE). Culture supernatants were then collected, centrifuged at 4°C at 1,600 rpm

893 for 8 minutes to allow removal of cell debris, aliquoted and stored at -80°C as the harvested viral
894 stock. Viral titers were determined in confluent monolayers of Vero E6 cells seeded in 96-well
895 plates using a 50% tissue culture infectious dose assay (TCID_{50}). Cells were infected with serial
896 1:10 dilutions (from 10^{-1} to 10^{-11}) of the virus and incubated at 37°C , in a humidified atmosphere
897 with 5% CO_2 . Plates were monitored daily for the presence of SARS-CoV-2 induced CPE for 4
898 days using an inverted optical microscope. The virus titer was estimated according to Spearman-
899 Karber formula (Kundi, 1999) and defined as the reciprocal of the highest viral dilution leading to at
900 least 50% CPE in inoculated wells.

901

902 **SARS-CoV-2 authentic virus neutralization assay**

903 All SARS-CoV-2 authentic virus neutralization assays were performed in the biosafety level 3
904 (BSL3) laboratories at Toscana Life Sciences in Siena (Italy) and Vismederi Srl, Siena (Italy). BSL3
905 laboratories are approved by a Certified Biosafety Professional and are inspected every year by
906 local authorities. The neutralization activity of culture supernatants from monoclonal was evaluated
907 using a CPE-based assay as previously described (Manenti et al., 2020). S-protein-specific
908 memory B cells produced antibodies were initially evaluated by means of a qualitative live-virus
909 based neutralization assay against a one-point dilution of the samples. Supernatants were mixed in
910 a 1:3 ratio with a SARS-CoV-2 viral solution containing 25 TCID_{50} of virus (final volume: 30 μL).
911 After 1 hour incubation at 37°C , 5% CO_2 , 25 μL of each virus-supernatant mixture was added to the
912 wells of a 96-well plate containing a sub-confluent Vero E6 cell monolayer. Following a 2-hours
913 incubation at 37°C , the virus-serum mixture was removed and 100 μL of DMEM 2% FBS were
914 added to each well. Plates were incubated for 3 days at 37°C in a humidified environment with 5%
915 CO_2 , then examined for CPE by means of an inverted optical microscope. Absence or presence of
916 CPE was defined by comparison of each well with the positive control (plasma sample showing
917 high neutralizing activity of SARS-CoV-2 in infected Vero E6 cells (Andreano et al., 2020) and
918 negative control (human serum sample negative for SARS-CoV-2 in ELISA and neutralization
919 assays). Following expression as full-length IgG1 recombinant antibodies were quantitatively
920 tested for their neutralization potency against both the wild type, D614G variant and the B.1.1.7

921 emerging variants. The assay was performed as previously described but using a viral titer of 100
922 TCID₅₀. Antibodies were prepared at a starting concentration of 20 µg/mL and diluted step 1:2.
923 Technical triplicates were performed for each experiment.

924

925 **Production and titration of SARS-CoV-2 pseudotyped lentiviral reporter particles**

926 Pseudotype stocks were prepared by FuGENE-HD (Promega) co-transfection of HEK293T/17 with
927 SARS-CoV-2 spike pcDNA3.1 + expression plasmid, HIV gag-pol p8.91 plasmid and firefly
928 luciferase expressing plasmid pCSFLW in a 1:0.8:1.2 ratio. 2×10^6 cells/cm² were plated 24h prior
929 to transfection in 10cm cell culture dishes. 48 and 72h post transfection, pseudotype-containing
930 culture medium was harvested and filtered through a 0.45µm syringe filter to clear cell debris.
931 Aliquots were stored at -80°C. Titration assays were performed by transduction of HEK293T/17
932 cells pre-transfected with ACE2 and TMPRSS2 plasmids to calculate the viral titer and infectious
933 dose (PV input) for neutralization assays. SARS-CoV-2 D614G pseudotype was produced using
934 the same procedure as described above. SARS-1 pseudotype was produced in a 1:0.5:0.8 ratio.
935 MERS-pseudotype was produced as previously described (Grehan et al., 2015).

936

937 **SARS-CoV-2 pseudotyped lentivirus neutralization assay**

938 The potency of the neutralizing mAbs was assessed using lentiviral particles expressing SARS-
939 CoV-2 spike protein on their surface and containing firefly luciferase as marker gene for detection
940 of infection. Briefly, 2×10^6 HEK293T cells were pre-transfected in a 10 cm dish the day before the
941 neutralization assay with ACE2 and TMPRSS2 plasmids in order to be used as optimal target cells
942 for SARS-CoV-2 PV entry. In a 96-well plate mAbs were 2-fold serially diluted in duplicate in culture
943 medium (DMEM supplemented with 10% fetal bovine serum and 1% penicillin/streptomycin)
944 starting at 20 µg/mL in a total volume of 100 µL. 1×10^6 RLU of SARS-CoV-2 pseudotyped lentiviral
945 particles were added to each well and incubated at 37°C for 1h. Each plate included PV plus cell
946 only (virus control) and cells only (background control). 1×10^4 pre-transfected HEK293T cells
947 suspended in 50 µL complete media were added per well and incubated for 48h at 37°C and 5%
948 CO₂. Firefly luciferase activity (luminescence) was measured using the Bright-Glo assay system
949 with a GloMax luminometer (Promega, UK). The raw Relative Luminescence Unit (RLU) data

950 points were converted to a percentage neutralization value, whereby 100% neutralization equals
951 the mean cell only RLU value control and 0% neutralization equals the mean PV only RLU value
952 control. The normalized data was then plotted using Prism 8 (GraphPad) on a neutralization
953 percentage scale and a NT50 value calculated, using the non-linear regression analysis. Plasma
954 from COVID-19 convalescent donors showing neutralization activity against SARS-CoV-2
955 (Andreano et al., 2020) were also assessed in this assay.

956

957 **Characterization of SARS-CoV-2 RBD-Antibodies binding by Flow cytometry**

958 Flow cytometry analysis was performed to define antibodies interaction with S-protein-receptor-
959 binding domain (RBD). Briefly, APEX™ Antibody Labeling Kits (Invitrogen) was used to conjugate
960 20 µg of selected antibodies to Alexa fluor 647, according to the manufacturer instructions. To
961 assess the ability of each antibody to bind the RBD domain, 1 mg of magnetic beads (Dynabeads™
962 His-Tag, Invitrogen) were coated with 70 µg of histidine tagged RBD, and then 20 µg/mL of each
963 labelled antibody were incubated with 40 µg/mL of beads-bound RBD for 1 hour on ice. Then,
964 samples were washed with 200 µL of Phosphate-buffered saline (PBS), resuspended in 150 µL of
965 PBS and assessed with a FACS Canto II flow cytometer (Becton Dickinson). Results were
966 analyzed by FlowJo (version 10).

967

968 **Flow Cytometry-Based S-protein Competition assay**

969 Antibodies specificity to bind SARS-CoV-2 S-protein and their possible competition was analyzed
970 performing a Flow cytometer-based assay. To this aim, 200 µg of stabilized histidine tagged S-
971 protein were coated with 1 mg of magnetic beads (Dynabeads™ His-Tag, Invitrogen). 20 µg of each
972 antibody were labelled with Alexa fluor 647 working with the APEX™ Antibody Labeling Kits
973 (Invitrogen). To test competitive binding profiles of the antibody panel selected, beads-bound S-
974 protein (40 µg/mL) were pre-incubated with unlabeled antibodies (40 µg/mL) for 1 hour on ice.
975 Then, each set of the beads-antibody complexes were washed with PBS and separately incubated
976 with each labelled antibody (20 µg/mL) for 1 hour on ice. After incubation, the mix Beads-antibodies
977 was washed, resuspended in 150 µL of PBS and analyzed using FACS Canto II flow cytometer
978 (Becton Dickinson). Beads-bound and non-bound S-protein incubated with labelled antibodies

979 were used as positive and negative control, respectively. Population gating and analysis was
980 carried out using FlowJo (version 10).

981

982 **Antigen-specific FcγR binding**

983 Fluorescently coded microspheres were used to profile the ability of selected antibodies to interact
984 with Fc receptors (Boudreau et al., 2020). The antigen of interest (SARS -CoV-2 S-protein RBD)
985 was covalently coupled to different bead sets via primary amine conjugation. The beads were
986 incubated with diluted antibody (diluted in PBS), allowing “on bead” affinity purification of antigen-
987 specific antibodies. The bound antibodies were subsequently probed with tetramerized
988 recombinant human FcγR2A and FcRN and analyzed using Luminex. The data is reported as the
989 median fluorescence intensity of PE for a specific bead channel.

990

991 **Antibody-dependent neutrophil phagocytosis**

992 Antibody-dependent neutrophil phagocytosis (ADNP) assesses the ability of antibodies to induce
993 the phagocytosis of antigen-coated targets by primary neutrophils. The assay was performed as
994 previously described (Karsten et al., 2019, Boudreau et al., 2020). Briefly, fluorescent streptavidin-
995 conjugated polystyrene beads were coupled to biotinylated SARS-CoV-2 Spike trimer. Diluted
996 antibody (diluted in PBS) was added, and unbound antibodies were washed away. The
997 antibody:bead complexes are added to primary neutrophils isolated from healthy blood donors
998 using negative selection (StemCell EasySep Direct Human Neutrophil Isolation Kit), and
999 phagocytosis was allowed to proceed for 1 hour. The cells were then washed and fixed, and the
1000 extent of phagocytosis was measured by flow cytometry. The data is reported as a phagocytic
1001 score, which considers the proportion of effector cells that phagocytosed and the degree of
1002 phagocytosis. Each sample is run in biological duplicate using neutrophils isolated from two distinct
1003 donors. The mAb were tested for ADNP activity at a range of 30 µg/mL to 137.17 ng/mL.

1004

1005 **Antibody-dependent NK cell activation**

1006 Antibody-dependent NK cell activation (ADNKA) assesses antigen-specific antibody-mediated NK
1007 cell activation against protein-coated plates. This assay was performed as previously described

1008 (Boudreau et al., 2020). Stabilized SARS-CoV-2 Spike trimer was used to coat ELISA plates, which
1009 were then washed and blocked. Diluted antibody (diluted in PBS) was added to the antigen coated
1010 plates, and unbound antibodies were washed away. NK cells, purified from healthy blood donor
1011 leukopaks using commercially available negative selection kits (StemCell EasySep Human NK Cell
1012 Isolation Kit) were added, and the levels of IFN- γ was measured after 5 hours using flow cytometry.
1013 The data is reported as the percent of cells positive for IFN- γ . Each sample is tested with at least
1014 two different NK cell donors, with all samples tested with each donor. The monoclonal antibodies
1015 were tested for ADNKA activity at a range of 20 $\mu\text{g}/\text{mL}$ to 9.1449 ng/mL.

1016

1017 **Affinity evaluation of SARS-CoV-2 neutralizing antibodies**

1018 Anti-Human IgG Polyclonal Antibody (Southern Biotech 2040-01) was immobilized via amine group
1019 on two flow cells of a CM5 sensor chip. For the immobilization, anti-human IgG Ab diluted in 10mM
1020 Na acetate pH 5.0 at the concentration of 25 $\mu\text{g}/\text{mL}$ was injected for 360 sec over the dextran
1021 matrix, which had been previously activated with a mixture of 0.1M 1-ethyl-3(3-
1022 dimethylaminopropyl)-carbodiimide (EDC) and 0.4 M N-hydroxyl succinimide (NHS) for 420 sec.
1023 After injection of the antibody, Ethanolamine 1M was injected to neutralize activated group. 10
1024 $\mu\text{L}/\text{min}$ flow rate was used during the whole procedure. Anti-SPIKE protein human mAbs were
1025 diluted in HBS-EP+ (Hepes 10 mM, NaCl 150 mM, EDTA 3.4 mM, 0.05% p20, pH 7.4) and injected
1026 for 120 sec at 10 $\mu\text{L}/\text{min}$ flow rate over one of the two flow cells containing the immobilized Anti-
1027 Human IgG Antibody, while running buffer (HBS-EP+) was injected over the other flow cell to be
1028 taken as blank. Dilution of each mAb was adjusted in order to have comparable levels of RU for
1029 each capture mAb. Following the capture of each mAb by the immobilized anti-human IgG
1030 antibody, different concentrations of SPIKE protein (20 $\mu\text{g}/\text{mL}$, 10 $\mu\text{g}/\text{mL}$, 5 $\mu\text{g}/\text{mL}$, 2.5 $\mu\text{g}/\text{mL}$ and 1
1031 $\mu\text{g}/\text{mL}$ in HBS-EP+) were injected over both the blank flow cell and the flow cell containing the
1032 captured mAb for 180 sec at a flow rate of 80 $\mu\text{L}/\text{min}$. Dissociation was followed for 800 sec,
1033 regeneration was achieved with a pulse (60 sec) of Glycine pH 1.5. Kinetic rates and affinity
1034 constant of SPIKE protein binding to each mAb were calculated applying a 1:1 binding as fitting
1035 model using the Bia T200 evaluation software 3.1.

1036

1037 Autoreactivity screening test on HEp-2 Cells

1038 The NOVA Lite HEp-2 ANA Kit (Inova Diagnostics) was used in accordance to the manufacturer's
1039 instructions to test antibodies the autoreactivity of selected antibodies which were tested at a
1040 concentration of 100 µg/mL. Kit positive and negative controls were used at three different dilutions
1041 (1:1, 1:10 and 1:100). Images were acquired using a DMI3000 B microscope (Leica) and an
1042 exposure time of 300 ms, channel intensity of 2000 and a gamma of 2.

1043

1044 Genetic Analyses of SARS-CoV-2 S-protein specific nAbs

1045 A custom pipeline was developed for the analyses of antibody sequences and the characterization
1046 of the immunoglobulin genes. Raw sequences were stored as ab1 file and transformed into fastaq
1047 using Biopython. The reads were then quality checked using FastQC
1048 (<https://www.bioinformatics.babraham.ac.uk/projects/fastqc/>) and a report was generated using
1049 MultiQC (<https://multiqc.info/>). The antibody leader sequence and the terminal part of the constant
1050 region were removed by trimming using Trimmomatic
1051 (<http://www.usadellab.org/cms/?page=trimmomatic>). This latter program was also used to scan and
1052 remove low-quality reads using a sliding-window parameter. Once sequences were recovered,
1053 germline gene assignment and annotation were performed with MiXCR
1054 (<https://mixcr.readthedocs.io/en/master/index.html>), using the single-read alignment parameters,
1055 and a CSV-formatted output was generated. Finally, the sequences retrieved from the antibodies
1056 described in this manuscript were compared to published neutralizing antibodies against SARS-
1057 CoV-2. For this purpose, the Coronavirus Antibody Database, CoV-AbDab
1058 (<http://opig.stats.ox.ac.uk/webapps/covabdab/>) was downloaded and the antibodies with reported
1059 neutralization activity against SARS-CoV-2 were extracted. Comparison analysis were performed
1060 in Python using NumPy (<https://numpy.org/>) and, Pandas (<https://pandas.pydata.org/>) while figures
1061 were produced using the Matplotlib tool (<https://matplotlib.org/>) and Seaborn
1062 (<https://seaborn.pydata.org/>).

1063

1064

1065 Negative-stain electron microscopy

1066 Complexes were formed by incubating SARS-2 CoV-GSAS-6P-Mut7 and respective fabs at a 1:3
1067 (trimer to fab) molar ratio for 30 minutes at room temperature. After diluting to 0.03 mg/ml in 1X
1068 TBS pH 7.4, the samples were deposited on plasma-cleaned copper mesh grids and stained with
1069 2% uranyl formate for 55 seconds. Automated data collection was made possible through the
1070 Leginon software (Suloway et al., 2005) and a FEI Tecnai Spirit (120keV, 56,000x mag) paired with
1071 a FEI Eagle (4k by 4k) CCD camera. Other details include a defocus value of -1.5 μm , a pixel size
1072 of 2.06 \AA per pixel, and a dose of 25 $e^-/\text{\AA}^2$. Raw micrographs were stored in the Appion database
1073 (Lander et al., 2009), particles were picked with DoGPicker (Voss et al., 2009), and 2D and 3D
1074 classification and refinements were performed in RELION 3.0 (Scheres, 2012). Map segmentation
1075 and model docking was done in UCSF Chimera (Pettersen et al., 2004).

1076

1077 Prophylactic and therapeutic passive transfer studies in golden Syrian hamsters

1078 Six- to eight-month-old female Syrian hamsters were purchased from Charles River Laboratories
1079 and housed in microisolator units, allowed free access to food and water and cared for under U.S.
1080 Department of Agriculture (USDA) guidelines for laboratory animals. For the passive transfer
1081 prophylactic experiments, the day prior to SARS-CoV-2 infection six hamsters per group were
1082 intraperitoneally administered with 500 μL of a 4, 1 or 0.25 mg/kg dose of J08-MUT mAb. For the
1083 passive transfer therapeutic experiments, the day after SARS-CoV-2 infection six hamsters per
1084 group were intraperitoneally administered with 500 μL of a 4 mg/kg dose of J08-MUT mAb. Another
1085 two groups (n=6/each) were administered with 500 μL of 4 mg/kg of the anti-influenza virus #1664
1086 human mAb (manuscript in preparation) or PBS only to serve as human IgG1 isotype and mock
1087 control groups, respectively. The day after, hamsters were anesthetized using 5% isoflurane, and
1088 inoculated with 5×10^5 PFU of SARS-CoV-2 (2019-nCoV/USA-WA1/2020) via the intranasal route,
1089 in a final volume of 100 μL . Baseline body weights were measured before infection as well as
1090 monitored daily for 7 and 11 days post infection in the prophylactic and therapeutic studies
1091 respectively. All experiments with the hamsters were performed in accordance with the NRC Guide
1092 for Care and Use of Laboratory Animals, the Animal Welfare act, and the CDC/NIH Biosafety and

1093 Microbiological and Biomedical Laboratories as well as the guidelines set by the Institutional
1094 Animal Care and Use Committee (IACUC) of the University of Georgia who also approved the
1095 animal experimental protocol. All animal studies infection with SARS-CoV-2 were conducted in the
1096 Animal Health Research Center (AHRC) Biosafety Level 3 (BSL-3) laboratories of the University of
1097 Georgia.

1098

1099 **Determination of viral load by TCID₅₀ assay**

1100 Lung tissues were homogenized in 1 mL of DMEM containing 1% fetal bovine serum (FBS) and 1%
1101 penicillin/streptomycin. The lung homogenate supernatant was diluted 10-fold (10^0 to 10^6) and
1102 used to determine median tissue culture infection dose (TCID₅₀) in Vero E6 cells as previously
1103 described (Jang and Ross, 2020).

1104

1105 **Human IgG detection in hamster sera**

1106 ELISA assay was used to detect the human IgG J08-MUT in hamster sera. 384-well plates (384
1107 well plates, Microplate Clear; Greiner Bio-one) were coated with 2 µg/mL of unlabeled goat anti-
1108 human IgG (SouthernBiotech) diluted in sterile PBS and incubated at 4°C overnight. 50 µL/well of
1109 saturation buffer (PBS/BSA 1%) was used to saturate unspecific binding and plates were incubated
1110 at 37°C for 1h without CO₂. Hamster sera were diluted in PBS/BSA 1%/Tween20 0.05% at a
1111 starting dilution of 1:10. Fourteen reciprocal dilutions were performed. Alkaline phosphatase-
1112 conjugated goat anti-human IgG (Sigma-Aldrich) was used as secondary antibody and pNPP (p-
1113 nitrophenyl phosphate) (Sigma-Aldrich) was used as soluble substrate. Wells were washed three
1114 times between each step with PBS/BSA 1%/Tween20 0.05%. The final reaction was measured by
1115 using the Varioskan Lux Reader (Thermo Fisher Scientific) at a wavelength of 405 nm. Samples
1116 were considered as positive if OD at 405 nm (OD₄₀₅) was twice the blank.

1117

1118 REFERENCES

- 1119 ACKERMAN, M. E., DUGAST, A.-S., MCANDREW, E. G., TSOUKAS, S., LICHT, A. F., IRVINE, D. J. & ALTER, G.
 1120 2013. Enhanced phagocytic activity of HIV-specific antibodies correlates with natural production of
 1121 immunoglobulins with skewed affinity for FcγR2a and FcγR2b. *Journal of virology*, 87, 5468-5476.
- 1122 ACKERMAN, M. E., MIKHAILOVA, A., BROWN, E. P., DOWELL, K. G., WALKER, B. D., BAILEY-KELLOGG, C.,
 1123 SUSCOVICH, T. J. & ALTER, G. 2016. Polyfunctional HIV-Specific Antibody Responses Are Associated
 1124 with Spontaneous HIV Control. *PLoS pathogens*, 12, e1005315-e1005315.
- 1125 ALSOUSSI, W. B., TURNER, J. S., CASE, J. B., ZHAO, H., SCHMITZ, A. J., ZHOU, J. Q., CHEN, R. E., LEI, T., RIZK,
 1126 A. A., MCINTIRE, K. M., WINKLER, E. S., FOX, J. M., KAFI, N. M., THACKRAY, L. B., HASSAN, A. O.,
 1127 AMANAT, F., KRAMMER, F., WATSON, C. T., KLEINSTEIN, S. H., FREMONT, D. H., DIAMOND, M. S. &
 1128 ELLEBEDY, A. H. 2020. A Potently Neutralizing Antibody Protects Mice against SARS-CoV-2 Infection.
 1129 *J Immunol*, 205, 915-922.
- 1130 ANDREANO, E., PICCINI, G., LICASTRO, D., CASALINO, L., JOHNSON, N. V., PACIELLO, I., MONEGO, S. D.,
 1131 PANTANO, E., MANGANARO, N., MANENTI, A., MANNA, R., CASA, E., HYSENI, I., BENINCASA, L.,
 1132 MONTOMOLI, E., AMARO, R. E., MCLELLAN, J. S. & RAPPUOLI, R. 2020. SARS-CoV-2 escape *in*
 1133 *vitro* from a highly neutralizing COVID-19 convalescent plasma. 2020.12.28.424451.
- 1134 ARATANI, L. 2020. Jobless America: the coronavirus unemployment crisis in figures. *The Guardian*.
- 1135 ARVIN, A. M., FINK, K., SCHMID, M. A., CATHCART, A., SPREAFICO, R., HAVENAR-DAUGHTON, C.,
 1136 LANZAVECCHIA, A., CORTI, D. & VIRGIN, H. W. 2020. A perspective on potential antibody-
 1137 dependent enhancement of SARS-CoV-2. *Nature*, 584, 353-363.
- 1138 BASTARD, P., ROSEN, L. B., ZHANG, Q., MICHAELIDIS, E., HOFFMANN, H. H., ZHANG, Y., DORGHAM, K.,
 1139 PHILIPPOT, Q., ROSAIN, J., BÉZIAT, V., MANRY, J., SHAW, E., HALJASMÄGI, L., PETERSON, P.,
 1140 LORENZO, L., BIZIEN, L., TROUILLET-ASSANT, S., DOBBS, K., DE JESUS, A. A., BELOT, A., KALLASTE, A.,
 1141 CATHERINOT, E., TANDJAOUI-LAMBIOTTE, Y., LE PEN, J., KERNER, G., BIGIO, B., SEELEUTHNER, Y.,
 1142 YANG, R., BOLZE, A., SPAAN, A. N., DELMONTE, O. M., ABERS, M. S., AIUTI, A., CASARI, G.,
 1143 LAMPASONA, V., PIEMONTE, L., CICERI, F., BILGUVAR, K., LIFTON, R. P., VASSE, M., SMADJA, D. M.,
 1144 MIGAUD, M., HADJADJ, J., TERRIER, B., DUFFY, D., QUINTANA-MURCI, L., VAN DE BEEK, D.,
 1145 ROUSSEL, L., VINH, D. C., TANGYE, S. G., HAERYNCK, F., DALMAU, D., MARTINEZ-PICADO, J.,
 1146 BRODIN, P., NUSSENZWEIG, M. C., BOISSON-DUPUIS, S., RODRÍGUEZ-GALLEGO, C., VOGT, G.,
 1147 MOGENSEN, T. H., OLER, A. J., GU, J., BURBELO, P. D., COHEN, J. I., BIONDI, A., BETTINI, L. R.,
 1148 D'ANGIO, M., BONFANTI, P., ROSSIGNOL, P., MAYAUX, J., RIEUX-LAUCAT, F., HUSEBYE, E. S., FUSCO,
 1149 F., URSINI, M. V., IMBERTI, L., SOTTINI, A., PAGHERA, S., QUIROS-ROLDAN, E., ROSSI, C.,
 1150 CASTAGNOLI, R., MONTAGNA, D., LICARI, A., MARSEGLIA, G. L., DUVAL, X., GHOSN, J., TSANG, J. S.,
 1151 GOLDBACH-MANSKY, R., KISAND, K., LIONAKIS, M. S., PUEL, A., ZHANG, S. Y., HOLLAND, S. M.,
 1152 GOROCHOV, G., JOUANGUY, E., RICE, C. M., COBAT, A., NOTARANGELO, L. D., ABEL, L., SU, H. C. &
 1153 CASANOVA, J. L. 2020. Autoantibodies against type I IFNs in patients with life-threatening COVID-
 1154 19. *Science*, 370.
- 1155 BAUM, A., AJITHDOSS, D., COPIN, R., ZHOU, A., LANZA, K., NEGRON, N., NI, M., WEI, Y., MOHAMMADI, K.,
 1156 MUSSER, B., ATWAL, G. S., OYEJIDE, A., GOEZ-GAZI, Y., DUTTON, J., CLEMMONS, E., STAPLES, H. M.,
 1157 BARTLEY, C., KLAFFKE, B., ALFSON, K., GAZI, M., GONZALEZ, O., DICK, E., JR., CARRION, R., JR.,
 1158 PESSAIN, L., PORTO, M., COOK, A., BROWN, R., ALI, V., GREENHOUSE, J., TAYLOR, T., ANDERSEN,
 1159 H., LEWIS, M. G., STAHL, N., MURPHY, A. J., YANCOPOULOS, G. D. & KYRATSOUS, C. A. 2020. REGN-
 1160 COV2 antibodies prevent and treat SARS-CoV-2 infection in rhesus macaques and hamsters.
 1161 *Science*.
- 1162 BOOTH, B. J., RAMAKRISHNAN, B., NARAYAN, K., WOLLACOTT, A. M., BABCOCK, G. J., SHRIVER, Z. &
 1163 VISWANATHAN, K. 2018. Extending human IgG half-life using structure-guided design. *mAbs*, 10,
 1164 1098-1110.
- 1165 BOUDREAU, C. M., YU, W.-H., SUSCOVICH, T. J., TALBOT, H. K., EDWARDS, K. M. & ALTER, G. 2020. Selective
 1166 induction of antibody effector functional responses using MF59-adjuvanted vaccination. *The*
 1167 *Journal of clinical investigation*, 130, 662-672.
- 1168 BUTLER, A. L., FALLON, J. K. & ALTER, G. 2019. A Sample-Sparing Multiplexed ADCP Assay. 10.

- 1169 CARNELL, G. W., FERRARA, F., GREHAN, K., THOMPSON, C. P. & TEMPERTON, N. J. 2015. Pseudotype-based
 1170 neutralization assays for influenza: a systematic analysis. *Front Immunol*, 6, 161.
- 1171 CARNELL, G. W., GREHAN, K., FERRARA, F., MOLESTI, E. & TEMPERTON, N. 2017. An Optimized Method for
 1172 the Production Using PEI, Titration and Neutralization of SARS-CoV Spike Luciferase Pseudotypes.
 1173 *Bio-protocol*, 7, e2514.
- 1174 CDC 2021. Emerging SARS-CoV-2 Variants.
- 1175 CHAKRABORTY, S., GONZALEZ, J., EDWARDS, K., MALLAJOSYULA, V., BUZZANCO, A. S., SHERWOOD, R.,
 1176 BUFFONE, C., KATHALE, N., PROVIDENZA, S., XIE, M. M., ANDREWS, J. R., BLISH, C. A., SINGH, U.,
 1177 DUGAN, H., WILSON, P. C., PHAM, T. D., BOYD, S. D., NADEAU, K. C., PINSKY, B. A., ZHANG, S.,
 1178 MEMOLI, M. J., TAUBENBERGER, J. K., MORALES, T., SCHAPIRO, J. M., TAN, G. S., JAGANNATHAN, P.
 1179 & WANG, T. T. 2020. Proinflammatory IgG Fc structures in patients with severe COVID-19. *Nat*
 1180 *Immunol*.
- 1181 CLAUSEN, T. M., SANDOVAL, D. R., SPLIID, C. B., PIHL, J., PAINTER, C. D., THACKER, B. E., GLASS, C. A.,
 1182 NARAYANAN, A., MAJOWICZ, S. A., ZHANG, Y., TORRES, J. L., GOLDEN, G. J., PORELL, R.,
 1183 GARRETSON, A. F., LAUBACH, L., FELDMAN, J., YIN, X., PU, Y., HAUSER, B., CARADONNA, T. M.,
 1184 KELLMAN, B. P., MARTINO, C., GORDTS, P. L. S. M., LEIBEL, S. L., CHANDA, S. K., SCHMIDT, A. G.,
 1185 GODULA, K., JOSE, J., CORBETT, K. D., WARD, A. B., CARLIN, A. F. & ESKO, J. D. 2020. SARS-CoV-2
 1186 Infection Depends on Cellular Heparan Sulfate and ACE2. *bioRxiv : the preprint server for biology*,
 1187 2020.07.14.201616.
- 1188 CUTLER, D. M. & SUMMERS, L. H. 2020. The COVID-19 Pandemic and the \$16 Trillion Virus. *Jama*, 324,
 1189 1495-1496.
- 1190 DILILLO, D. J., TAN, G. S., PALESE, P. & RAVETCH, J. V. 2014. Broadly neutralizing hemagglutinin stalk-specific
 1191 antibodies require FcγR interactions for protection against influenza virus in vivo. *Nat Med*, 20, 143-
 1192 51.
- 1193 FDA 2020. Coronavirus (COVID-19) Update: FDA Authorizes Monoclonal Antibodies for Treatment of
 1194 COVID-19.
- 1195 FDA 2021. COVID-19 Vaccines.
- 1196 GAUDINSKI, M. R., COATES, E. E., HOUSER, K. V., CHEN, G. L., YAMSHCHIKOV, G., SAUNDERS, J. G.,
 1197 HOLMAN, L. A., GORDON, I., PLUMMER, S., HENDEL, C. S., CONAN-CIBOTTI, M., LORENZO, M. G.,
 1198 SITAR, S., CARLTON, K., LAURENCOT, C., BAILER, R. T., NARPALA, S., MCDERMOTT, A. B.,
 1199 NAMBOODIRI, A. M., PANDEY, J. P., SCHWARTZ, R. M., HU, Z., KOUP, R. A., CAPPARELLI, E.,
 1200 GRAHAM, B. S., MASCOLA, J. R. & LEDGERWOOD, J. E. 2018. Safety and pharmacokinetics of the Fc-
 1201 modified HIV-1 human monoclonal antibody VRC01LS: A Phase 1 open-label clinical trial in healthy
 1202 adults. *PLoS Med*, 15, e1002493.
- 1203 GREHAN, K., FERRARA, F. & TEMPERTON, N. 2015. An optimised method for the production of MERS-CoV
 1204 spike expressing viral pseudotypes. *MethodsX*, 2, 379-84.
- 1205 GRIFFIN, M. P., YUAN, Y., TAKAS, T., DOMACHOWSKIE, J. B., MADHI, S. A., MANZONI, P., SIMÕES, E. A. F.,
 1206 ESSER, M. T., KHAN, A. A., DUBOVSKY, F., VILLAFANA, T. & DEVINCENZO, J. P. 2020. Single-Dose
 1207 Nirsevimab for Prevention of RSV in Preterm Infants. *N Engl J Med*, 383, 415-425.
- 1208 HANSEN, J., BAUM, A., PASCAL, K. E., RUSSO, V., GIORDANO, S., WLOGA, E., FULTON, B. O., YAN, Y., KOON,
 1209 K., PATEL, K., CHUNG, K. M., HERMANN, A., ULLMAN, E., CRUZ, J., RAFIQUE, A., HUANG, T.,
 1210 FAIRHURST, J., LIBERTINY, C., MALBEC, M., LEE, W.-Y., WELSH, R., FARR, G., PENNINGTON, S.,
 1211 DESHPANDE, D., CHENG, J., WATTY, A., BOUFFARD, P., BABB, R., LEVENKOVA, N., CHEN, C., ZHANG,
 1212 B., ROMERO HERNANDEZ, A., SAOTOME, K., ZHOU, Y., FRANKLIN, M., SIVAPALASINGAM, S., LYE, D.
 1213 C., WESTON, S., LOGUE, J., HAUPT, R., FRIEMAN, M., CHEN, G., OLSON, W., MURPHY, A. J., STAHL,
 1214 N., YANCOPOULOS, G. D. & KYRATSOUS, C. A. 2020. Studies in humanized mice and convalescent
 1215 humans yield a SARS-CoV-2 antibody cocktail. *Science (New York, N.Y.)*, 369, 1010-1014.
- 1216 HOOFT VAN HUIJSDUIJNEN, R., KOJIMA, S., CARTER, D., OKABE, H., SATO, A., AKAHATA, W., WELLS, T. N. C.
 1217 & KATSUNO, K. 2020. Reassessing therapeutic antibodies for neglected and tropical diseases. *PLoS*
 1218 *neglected tropical diseases*, 14, e0007860-e0007860.
- 1219 HSIEH, C. L., GOLDSMITH, J. A., SCHAUB, J. M., DIVENERE, A. M., KUO, H. C., JAVANMARDI, K., LE, K. C.,
 1220 WRAPP, D., LEE, A. G., LIU, Y., CHOU, C. W., BYRNE, P. O., HJORTH, C. K., JOHNSON, N. V., LUDES-

- 1221 MEYERS, J., NGUYEN, A. W., PARK, J., WANG, N., AMENGOR, D., LAVINDER, J. J., IPPOLITO, G. C.,
1222 MAYNARD, J. A., FINKELSTEIN, I. J. & MCLELLAN, J. S. 2020. Structure-based design of prefusion-
1223 stabilized SARS-CoV-2 spikes. *Science*, 369, 1501-1505.
- 1224 HUANG, J., DORIA-ROSE, N. A., LONGO, N. S., LAUB, L., LIN, C. L., TURK, E., KANG, B. H., MIGUELES, S. A.,
1225 BAILER, R. T., MASCOLA, J. R. & CONNORS, M. 2013. Isolation of human monoclonal antibodies
1226 from peripheral blood B cells. *Nat Protoc*, 8, 1907-15.
- 1227 IMAI, M., IWATSUKI-HORIMOTO, K., HATTA, M., LOEBER, S., HALFMANN, P. J., NAKAJIMA, N., WATANABE,
1228 T., UJIE, M., TAKAHASHI, K., ITO, M., YAMADA, S., FAN, S., CHIBA, S., KURODA, M., GUAN, L.,
1229 TAKADA, K., ARMBRUST, T., BALOGH, A., FURUSAWA, Y., OKUDA, M., UEKI, H., YASUHARA, A.,
1230 SAKAI-TAGAWA, Y., LOPES, T. J. S., KISO, M., YAMAYOSHI, S., KINOSHITA, N., OHMAGARI, N.,
1231 HATTORI, S.-I., TAKEDA, M., MITSUYA, H., KRAMMER, F., SUZUKI, T. & KAWAOKA, Y. 2020. Syrian
1232 hamsters as a small animal model for SARS-CoV-2 infection and countermeasure development. 117,
1233 16587-16595.
- 1234 JANG, H. & ROSS, T. M. 2020. Dried SARS-CoV-2 virus maintains infectivity to Vero E6 cells for up to 48 h.
1235 *Vet Microbiol*, 251, 108907.
- 1236 KANEKO, N., KUO, H.-H., BOUCAU, J., FARMER, J. R., ALLARD-CHAMARD, H., MAHAJAN, V. S., PIECHOCKA-
1237 TROCHA, A., LEFTEI, K., OSBORN, M., BALS, J., BARTSCH, Y. C., BONHEUR, N., CARADONNA, T. M.,
1238 CHEVALIER, J., CHOWDHURY, F., DIEFENBACH, T. J., EINKAUF, K., FALLON, J., FELDMAN, J., FINN, K.
1239 K., GARCIA-BRONCANO, P., HARTANA, C. A., HAUSER, B. M., JIANG, C., KAPLONEK, P., KARPELL, M.,
1240 KOSCHER, E. C., LIAN, X., LIU, H., LIU, J., LY, N. L., MICHELL, A. R., RASSADKINA, Y., SEIGER, K., SESSA,
1241 L., SHIN, S., SINGH, N., SUN, W., SUN, X., TICHELI, H. J., WARING, M. T., ZHU, A. L., LI, J., LINGWOOD,
1242 D., SCHMIDT, A. G., LICHTERFELD, M., WALKER, B. D., YU, X., PADERA, R. F., JR., PILLAI, S. &
1243 MASSACHUSETTS CONSORTIUM ON PATHOGEN READINESS SPECIMEN WORKING, G. 2020. The
1244 Loss of Bcl-6 Expressing T Follicular Helper Cells and the Absence of Germinal Centers in COVID-19.
1245 *SSRN*, 3652322-3652322.
- 1246 KARSTEN, C. B., MEHTA, N., SHIN, S. A., DIEFENBACH, T. J., SLEIN, M. D., KARPINSKI, W., IRVINE, E. B.,
1247 BROGE, T., SUSCOVICH, T. J. & ALTER, G. 2019. A versatile high-throughput assay to characterize
1248 antibody-mediated neutrophil phagocytosis. *Journal of immunological methods*, 471, 46-56.
- 1249 KATZELNICK, L. C., GRESH, L., HALLORAN, M. E., MERCADO, J. C., KUAN, G., GORDON, A., BALMASEDA, A. &
1250 HARRIS, E. 2017. Antibody-dependent enhancement of severe dengue disease in humans. *Science*,
1251 358, 929-932.
- 1252 KELLEY, B. 2020. Developing therapeutic monoclonal antibodies at pandemic pace. *Nat Biotechnol*.
- 1253 KORBER, B., FISCHER, W. M., GNANAKARAN, S., YOON, H., THEILER, J., ABFALTERER, W., HENGARTNER, N.,
1254 GIORGI, E. E., BHATTACHARYA, T., FOLEY, B., HASTIE, K. M., PARKER, M. D., PARTRIDGE, D. G.,
1255 EVANS, C. M., FREEMAN, T. M., DE SILVA, T. I., SHEFFIELD, C.-G. G., MCDANAL, C., PEREZ, L. G.,
1256 TANG, H., MOON-WALKER, A., WHELAN, S. P., LABRANCHE, C. C., SAPHIRE, E. O. & MONTEFIORI, D.
1257 C. 2020. Tracking Changes in SARS-CoV-2 Spike: Evidence that D614G Increases Infectivity of the
1258 COVID-19 Virus. *Cell*, S0092-8674(20)30820-5.
- 1259 KREER, C., ZEHNER, M., WEBER, T., ERCANOGLU, M. S., GIESELMANN, L., ROHDE, C., HALWE, S., KORENKOV,
1260 M., SCHOMMERS, P., VANSHYLLA, K., DI CRISTANZIANO, V., JANICKI, H., BRINKER, R., ASHUROV, A.,
1261 KRÄHLING, V., KUPKE, A., COHEN-DVASHI, H., KOCH, M., ECKERT, J. M., LEDERER, S., PFEIFER, N.,
1262 WOLF, T., VEHRSCCHILD, M., WENDTNER, C., DISKIN, R., GRUELL, H., BECKER, S. & KLEIN, F. 2020.
1263 Longitudinal Isolation of Potent Near-Germline SARS-CoV-2-Neutralizing Antibodies from COVID-19
1264 Patients. *Cell*, 182, 843-854.e12.
- 1265 KREYE, J., REINCKE, S. M., KORNAU, H.-C., SÁNCHEZ-SENDIN, E., CORMAN, V. M., LIU, H., YUAN, M., WU, N.
1266 C., ZHU, X., LEE, C.-C. D., TRIMPERT, J., HÖLTJE, M., DIETERT, K., STÖFFLER, L., VON WARDENBURG,
1267 N., VAN HOOF, S., HOMEYER, M. A., HOFFMANN, J., ABDELGAWAD, A., GRUBER, A. D., BERTZBACH,
1268 L. D., VLADIMIROVA, D., LI, L. Y., BARTHEL, P. C., SKRINER, K., HOCKE, A. C., HIPPENSTIEL, S.,
1269 WITZENRATH, M., SUTTORP, N., KURTH, F., FRANKE, C., ENDRES, M., SCHMITZ, D., JEWOROWSKI, L.
1270 M., RICHTER, A., SCHMIDT, M. L., SCHWARZ, T., MÜLLER, M. A., DROSTEN, C., WENDISCH, D.,
1271 SANDER, L. E., OSTERRIEDER, N., WILSON, I. A. & PRÜSS, H. 2020. A Therapeutic Non-self-reactive

- 1272 SARS-CoV-2 Antibody Protects from Lung Pathology in a COVID-19 Hamster Model. *Cell*, 183, 1058-
1273 1069.e19.
- 1274 KUNDI, M. 1999. One-hit models for virus inactivation studies. *Antiviral Res*, 41, 145-52.
- 1275 KUPFFERSCHMIDT, K. 2019. Successful Ebola treatments promise to tame outbreak. *Science*, 365, 628-629.
- 1276 LANDER, G. C., STAGG, S. M., VOSS, N. R., CHENG, A., FELLMANN, D., PULOKAS, J., YOSHIOKA, C., IRVING, C.,
1277 MULDER, A., LAU, P.-W., LYUMKIS, D., POTTER, C. S. & CARRAGHER, B. 2009. Appion: an integrated,
1278 database-driven pipeline to facilitate EM image processing. *Journal of structural biology*, 166, 95-
1279 102.
- 1280 LEE, W. S., WHEATLEY, A. K., KENT, S. J. & DEKOSKY, B. J. 2020. Antibody-dependent enhancement and
1281 SARS-CoV-2 vaccines and therapies. *Nat Microbiol*, 5, 1185-1191.
- 1282 LILLY 2020. Lilly's neutralizing antibody bamlanivimab (LY-CoV555) receives FDA emergency use
1283 authorization for the treatment of recently diagnosed COVID-19.
- 1284 LIU, L., WANG, P., NAIR, M. S., YU, J., RAPP, M., WANG, Q., LUO, Y., CHAN, J. F. W., SAHI, V., FIGUEROA, A.,
1285 GUO, X. V., CERUTTI, G., BIMELA, J., GORMAN, J., ZHOU, T., CHEN, Z., YUEN, K.-Y., KWONG, P. D.,
1286 SODROSKI, J. G., YIN, M. T., SHENG, Z., HUANG, Y., SHAPIRO, L. & HO, D. D. 2020. Potent
1287 neutralizing antibodies against multiple epitopes on SARS-CoV-2 spike. *Nature*, 584, 450-456.
- 1288 MACKNESS, B. C., JAWORSKI, J. A., BOUDANOVA, E., PARK, A., VALENTE, D., MAURIAC, C., PASQUIER, O.,
1289 SCHMIDT, T., KABIRI, M., KANDIRA, A., RADOŠEVIĆ, K. & QIU, H. 2019. Antibody Fc engineering for
1290 enhanced neonatal Fc receptor binding and prolonged circulation half-life. *mAbs*, 11, 1276-1288.
- 1291 MANENTI, A., MAGGETTI, M., CASA, E., MARTINUZZI, D., TORELLI, A., TROMBETTA, C. M., MARCHI, S. &
1292 MONTOMOLI, E. 2020. Evaluation of SARS-CoV-2 neutralizing antibodies using a CPE-based
1293 colorimetric live virus micro-neutralization assay in human serum samples. *J Med Virol*.
- 1294 MULLARD, A. 2020. FDA approves antibody cocktail for Ebola virus. *Nat Rev Drug Discov*.
- 1295 PEGU, A., HESSELL, A. J., MASCOLA, J. R. & HAIGWOOD, N. L. 2017. Use of broadly neutralizing antibodies
1296 for HIV-1 prevention. *Immunological reviews*, 275, 296-312.
- 1297 PETERSEN, E. F., GODDARD, T. D., HUANG, C. C., COUCH, G. S., GREENBLATT, D. M., MENG, E. C. & FERRIN,
1298 T. E. 2004. UCSF Chimera--a visualization system for exploratory research and analysis. *J Comput
1299 Chem*, 25, 1605-12.
- 1300 PINTO, D., PARK, Y. J., BELTRAMELLO, M., WALLS, A. C., TORTORICI, M. A., BIANCHI, S., JACONI, S., CULAP,
1301 K., ZATTA, F., DE MARCO, A., PETER, A., GUARINO, B., SPREAFICO, R., CAMERONI, E., CASE, J. B.,
1302 CHEN, R. E., HAVENAR-DAUGHTON, C., SNELL, G., TELENTI, A., VIRGIN, H. W., LANZAVECCHIA, A.,
1303 DIAMOND, M. S., FINK, K., VEESLER, D. & CORTI, D. 2020. Cross-neutralization of SARS-CoV-2 by a
1304 human monoclonal SARS-CoV antibody. *Nature*, 583, 290-295.
- 1305 REGENERON 2020. REGENERON'S CASIRIVIMAB AND IMDEVIMAB ANTIBODY COCKTAIL FOR COVID-19 IS
1306 FIRST COMBINATION THERAPY TO RECEIVE FDA EMERGENCY USE AUTHORIZATION.
- 1307 ROGERS, T. F., ZHAO, F., HUANG, D., BEUTLER, N., BURNS, A., HE, W.-T., LIMBO, O., SMITH, C., SONG, G.,
1308 WOEHL, J., YANG, L., ABBOTT, R. K., CALLAGHAN, S., GARCIA, E., HURTADO, J., PARREN, M., PENG,
1309 L., RAMIREZ, S., RICKETTS, J., RICCIARDI, M. J., RAWLINGS, S. A., WU, N. C., YUAN, M., SMITH, D. M.,
1310 NEMAZEE, D., TEIJARO, J. R., VOSS, J. E., WILSON, I. A., ANDRABI, R., BRINEY, B., LANDAIS, E., SOK,
1311 D., JARDINE, J. G. & BURTON, D. R. 2020. Isolation of potent SARS-CoV-2 neutralizing antibodies and
1312 protection from disease in a small animal model. *Science (New York, N.Y.)*, 369, 956-963.
- 1313 ROMANO, M., RUGGIERO, A., SQUEGLIA, F., MAGA, G. & BERISIO, R. 2020. A Structural View of SARS-CoV-2
1314 RNA Replication Machinery: RNA Synthesis, Proofreading and Final Capping. *Cells*, 9, 1267.
- 1315 SCHÄFER, A., MUECKSCH, F., LORENZI, J. C. C., LEIST, S. R., CIPOLLA, M., BOURNAZOS, S., SCHMIDT, F.,
1316 GAZUMYAN, A., BARIC, R. S., ROBBIANI, D. F., HATZIOANNOU, T., RAVETCH, J. V., BIENIASZ, P. D.,
1317 NUSSENZWEIG, M. C. & SHEAHAN, T. P. 2020. Antibody potency, effector function and
1318 combinations in protection from SARS-CoV-2 infection in vivo. *bioRxiv : the preprint server for
1319 biology*, 2020.09.15.298067.
- 1320 SCHERES, S. H. 2012. RELION: implementation of a Bayesian approach to cryo-EM structure determination.
1321 *J Struct Biol*, 180, 519-30.

- 1322 SCHLOTHAUER, T., HERTER, S., KOLLER, C. F., GRAU-RICHARDS, S., STEINHART, V., SPICK, C., KUBBIES, M.,
 1323 KLEIN, C., UMAÑA, P. & MÖSSNER, E. 2016. Novel human IgG1 and IgG4 Fc-engineered antibodies
 1324 with completely abolished immune effector functions. *Protein Eng Des Sel*, 29, 457-466.
- 1325 SHI, R., SHAN, C., DUAN, X., CHEN, Z., LIU, P., SONG, J., SONG, T., BI, X., HAN, C., WU, L., GAO, G., HU, X.,
 1326 ZHANG, Y., TONG, Z., HUANG, W., LIU, W. J., WU, G., ZHANG, B., WANG, L., QI, J., FENG, H., WANG,
 1327 F. S., WANG, Q., GAO, G. F., YUAN, Z. & YAN, J. 2020. A human neutralizing antibody targets the
 1328 receptor-binding site of SARS-CoV-2. *Nature*, 584, 120-124.
- 1329 SIA, S. F., YAN, L. M., CHIN, A. W. H., FUNG, K., CHOY, K. T., WONG, A. Y. L., KAEWPREEDEE, P., PERERA, R.,
 1330 POON, L. L. M., NICHOLLS, J. M., PEIRIS, M. & YEN, H. L. 2020. Pathogenesis and transmission of
 1331 SARS-CoV-2 in golden hamsters. *Nature*, 583, 834-838.
- 1332 SPARROW, E., FRIEDE, M., SHEIKH, M. & TORVALDSEN, S. 2017. Therapeutic antibodies for infectious
 1333 diseases. *Bulletin of the World Health Organization*, 95, 235-237.
- 1334 SULOWAY, C., PULOKAS, J., FELLMANN, D., CHENG, A., GUERRA, F., QUISPE, J., STAGG, S., POTTER, C. S. &
 1335 CARRAGHER, B. 2005. Automated molecular microscopy: the new Legimon system. *J Struct Biol*,
 1336 151, 41-60.
- 1337 TAY, M. Z., POH, C. M., RENIA, L., MACARY, P. A. & NG, L. F. P. 2020. The trinity of COVID-19: immunity,
 1338 inflammation and intervention. *Nat Rev Immunol*.
- 1339 TILLER, T., MEFFRE, E., YURASOV, S., TSUIJI, M., NUSSENZWEIG, M. C. & WARDEMANN, H. 2008. Efficient
 1340 generation of monoclonal antibodies from single human B cells by single cell RT-PCR and expression
 1341 vector cloning. *Journal of immunological methods*, 329, 112-124.
- 1342 VOSS, N. R., YOSHIOKA, C. K., RADERMACHER, M., POTTER, C. S. & CARRAGHER, B. 2009. DoG Picker and
 1343 TiltPicker: software tools to facilitate particle selection in single particle electron microscopy. *J*
 1344 *Struct Biol*, 166, 205-13.
- 1345 WALLS, A. C., PARK, Y. J., TORTORICI, M. A., WALL, A., MCGUIRE, A. T. & VEESLER, D. 2020. Structure,
 1346 Function, and Antigenicity of the SARS-CoV-2 Spike Glycoprotein. *Cell*, 181, 281-292.e6.
- 1347 WANG, Q., ZHANG, Y., WU, L., NIU, S., SONG, C., ZHANG, Z., LU, G., QIAO, C., HU, Y., YUEN, K. Y., WANG, Q.,
 1348 ZHOU, H., YAN, J. & QI, J. 2020. Structural and Functional Basis of SARS-CoV-2 Entry by Using
 1349 Human ACE2. *Cell*.
- 1350 WARDEMANN, H. & BUSSE, C. E. 2019. Expression Cloning of Antibodies from Single Human B Cells.
 1351 *Methods Mol Biol*, 1956, 105-125.
- 1352 WELLCOME 2020. Expanding access to monoclonal antibody-based products: a global call to action.
- 1353 WRAPP, D., WANG, N., CORBETT, K. S., GOLDSMITH, J. A., HSIEH, C. L., ABIONA, O., GRAHAM, B. S. &
 1354 MCLELLAN, J. S. 2020. Cryo-EM structure of the 2019-nCoV spike in the prefusion conformation.
 1355 *Science*, 367, 1260-1263.
- 1356 YUAN, M., LIU, H., WU, N. C., LEE, C.-C. D., ZHU, X., ZHAO, F., HUANG, D., YU, W., HUA, Y., TIEN, H., ROGERS,
 1357 T. F., LANDAIS, E., SOK, D., JARDINE, J. G., BURTON, D. R. & WILSON, I. A. 2020. Structural basis of a
 1358 public antibody response to SARS-CoV-2. *bioRxiv : the preprint server for biology*,
 1359 2020.06.08.141267.
- 1360 ZALEVSKY, J., CHAMBERLAIN, A. K., HORTON, H. M., KARKI, S., LEUNG, I. W. L., SPROULE, T. J., LAZAR, G. A.,
 1361 ROOPENIAN, D. C. & DESJARLAIS, J. R. 2010. Enhanced antibody half-life improves in vivo activity.
 1362 *Nature biotechnology*, 28, 157-159.
- 1363 ZOST, S. J., GILCHUK, P., CASE, J. B., BINSSTEIN, E., CHEN, R. E., NKOLOLA, J. P., SCHÄFER, A., REIDY, J. X.,
 1364 TRIVETTE, A., NARGI, R. S., SUTTON, R. E., SURYADEVARA, N., MARTINEZ, D. R., WILLIAMSON, L. E.,
 1365 CHEN, E. C., JONES, T., DAY, S., MYERS, L., HASSAN, A. O., KAFI, N. M., WINKLER, E. S., FOX, J. M.,
 1366 SHRIHARI, S., MUELLER, B. K., MEILER, J., CHANDRASHEKAR, A., MERCADO, N. B., STEINHARDT, J. J.,
 1367 REN, K., LOO, Y. M., KALLEWAARD, N. L., MCCUNE, B. T., KEELER, S. P., HOLTZMAN, M. J.,
 1368 BAROUCH, D. H., GRALINSKI, L. E., BARIC, R. S., THACKRAY, L. B., DIAMOND, M. S., CARNAHAN, R. H.
 1369 & CROWE, J. E., JR. 2020a. Potently neutralizing and protective human antibodies against SARS-
 1370 CoV-2. *Nature*, 584, 443-449.
- 1371 ZOST, S. J., GILCHUK, P., CHEN, R. E., CASE, J. B., REIDY, J. X., TRIVETTE, A., NARGI, R. S., SUTTON, R. E.,
 1372 SURYADEVARA, N., CHEN, E. C., BINSSTEIN, E., SHRIHARI, S., OSTROWSKI, M., CHU, H. Y., DIDIER, J.
 1373 E., MACRENARIS, K. W., JONES, T., DAY, S., MYERS, L., EUN-HYUNG LEE, F., NGUYEN, D. C., SANZ, I.,

- 1374 MARTINEZ, D. R., ROTHLAUF, P. W., BLOYET, L. M., WHELAN, S. P. J., BARIC, R. S., THACKRAY, L. B.,
1375 DIAMOND, M. S., CARNAHAN, R. H. & CROWE, J. E., JR. 2020b. Rapid isolation and profiling of a
1376 diverse panel of human monoclonal antibodies targeting the SARS-CoV-2 spike protein. *Nat Med*,
1377 26, 1422-1427.
- 1378 ZOU, X., CHEN, K., ZOU, J., HAN, P., HAO, J. & HAN, Z. 2020. Single-cell RNA-seq data analysis on the
1379 receptor ACE2 expression reveals the potential risk of different human organs vulnerable to 2019-
1380 nCoV infection. *Front Med*.
- 1381 ZUO, Y., ESTES, S. K., ALI, R. A., GANDHI, A. A., YALAVARTHI, S., SHI, H., SULE, G., GOCKMAN, K., MADISON, J.
1382 A., ZUO, M., YADAV, V., WANG, J., WOODARD, W., LEZAK, S. P., LUGOGO, N. L., SMITH, S. A.,
1383 MORRISSEY, J. H., KANTHI, Y. & KNIGHT, J. S. 2020. Prothrombotic autoantibodies in serum from
1384 patients hospitalized with COVID-19. *Sci Transl Med*.

Journal Pre-proof

IN BRIEF

Extremely potent neutralizing human monoclonal antibodies, though rare, are isolated from COVID-19 convalescent patients and suitable for prophylactic and therapeutic interventions of wild type SARS-CoV-2 as well as emerging variants.

HIGHLIGHTS

- Human memory B cells encoding extremely potent neutralizing antibodies are rare.
- Most potent antibodies recognize the tip of the spike receptor binding domain.
- Selected neutralizing antibody neutralizes SARS-CoV-2 emerging variants.
- Potent antibody prevents and treats hamster infection without Fc-functions

